Imperial College London

Imperial College London

Department of Mathematics

Study of the joint S&P 500/VIX smile calibration problem within rough volatility models

Author: Pierre-Alexis CORPECHOT (CID: 01791800)

A thesis submitted for the degree of

MSc in Mathematics and Finance, 2019-2020

Declaration

The work contained in this thesis is my own work unless otherwise stated.

Acknowledgements

First of all, I would like to express my gratitude to my master thesis supervisor Dr. Antoine Jacquier for introducing me to this challenging topic that is rough volatility. His continued support and guidance were very helpful to conduct all these researches successfully.

I would like also to thank the whole team of the MSc Mathematics and Finance at Imperial College for the richness of the teaching they offered. It was definitely a stimulating and rewarding experience.

I am also very grateful to my mother, my father, my sister and my grandparents for their unconditional love and support throughout those years of studies.

Finally, this journey would not have been possible without the unfailling patience and love of Laura. There are no words to express how I am grateful to her and my family.

Abstract

The rough nature of the volatility process is now widely accepted in quantitative finance. Statistical analysis like [1] and [2] shed light on rough volatility models, where the volatility process is driven by a fractional Brownian motion with Hurst exponent of order 0.1, ignoring therefore the long memory feature that motivated Comte and Renault to consider such dynamics in [3] more than twenty years ago. Rough volatility models are able to capture and explain stylized facts observed from historical market data in volatility time series and in the implied volatility of option prices.

Throughout this paper, we study revisited pricing models under rough volatility dynamics and their possible applications to the joint S&P 500/VIX smile calibration problem. But due to the non-Markovian nature of the fractional Brownian motion, numerical implementations of those pricing models are computationally more expensive.

The hybrid scheme introduced by Bennedsen in [4] was implemented to simulate efficiently the rough Bergomi model, which provides good fits to the SPX implied volatility smiles, but it is not consistent with the VIX options market. Then, regarding the generalized rough Heston model, we used the Adams numerical scheme to simulate the characteristic function of the log-price which is the solution of a fractional Ricatti equation. Afterwards, the inverse Fourier transform is applied to get the price of European Call options. The fits to SPX and VIX smiles are good, but the joint calibration was not possible. Finally, only the quadratic rough Heston simulated with the hybrid scheme offers an acceptable joint calibration between SPX and VIX.

Contents

List of Figures

List of Tables

Introduction

Over the last decade, volatility modeling has become a major challenge in quantitative finance. Although volatility is not directly observed on financial markets, it is now the subject of many research papers to estimate it and to use it for trading strategies.

In the financial world, log-prices are, most of the time, modeled as continuous semi-martingale. Therefore, for a given asset with log-price process $(Y_t)_{t\geq 0}$, the dynamics could be written as follows:

$$dY_t = \nu_t dt + \sigma_t dW_t, \tag{0.0.1}$$

with $(\sigma_t)_{t\geq 0}$ the volatility process. In the well-known Black-Scholes pricing model, the volatility process is constant and deterministic. But since the implied volatility surface observed from historical market data is not flat (see Figures (1.1) and (1.3)), the assumptions regarding the volatility process cannot be considered relevant any longer. So, a popular approach is to model volatility as a stochastic process where the choice of the specific dynamics defines the model (like the Hull and White model, the Heston model, the SABR model etc).

Since the publication of statistical analysis of realized volatility by Jim Gatheral et al. in [1] and the theoretical results on implied volatility obtained by Elisa Alòs et al. in [2] and by Fukasawa in [5], rough volatility models have gained in popularity. These models are characterized by the presence of a stochastic process rougher than Brownian motion that drives the volatility process. More precisely, this "*rougher*" stochastic process is a fractional Brownian motion with Hurst index $H \in]0, 1[$, see Appendix (E.1).

Such models were first introduced by Comte and Renault in [3]. They assumed the volatility process to be not only stochastic but also to have long-memory features and properties. Then they proposed to model log-volatility using a fractional Brownian motion with $H > 1/2$ to ensure that volatility is a long-memory process.

Nevertheless, by considering a volatility process driven by a fractional Brownian motion with $H < 1/2$, Jim Gatheral and Fukasawa with their respective paper [1] and [5] showed that rough volatility models are able to capture and explain stylized facts observed from historical market data in volatility time series and in the implied volatility of option prices. Furthermore, several research papers demonstrate the ability of those models, under revisited classical pricing models, to fit the implied volatility smiles in Equity markets for short maturities, where continuous Markovian stochastic volatility models fail to describe. But numerical implementations of those pricing models are computationally more expensive due to the non-Markovian nature of the fractional Brownian motion. Hence, efficient pricing methods are required to perform calibrations and simulations.

Since the fits to implied volatility surfaces are promising, rough volatility models open the door to calibration problems as well, including the most well-known and the most challenging problem in volatility modelling, the joint S&P 500/ VIX smile calibration problem.

The volatility index, or VIX, is based on the S&P 500 index (SPX) options. It is also known as the *fear index* and it represents a popular measure of the expected volatility over the next 30 days of the stock market.

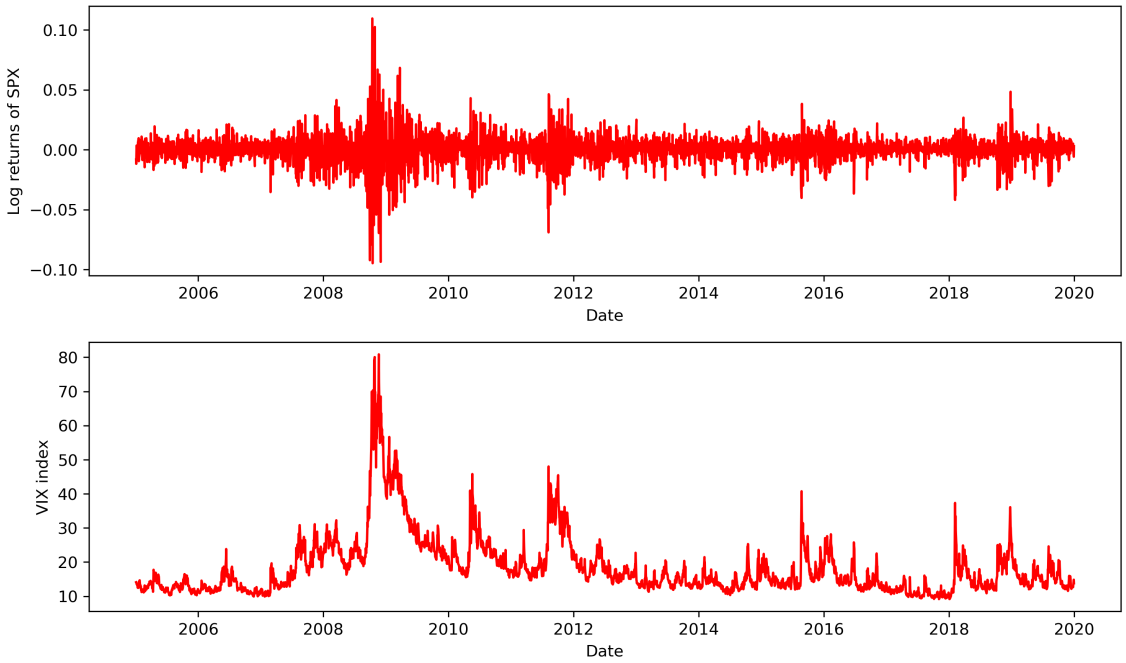

Figure 1: Log-returns of SPX (above) and VIX index (below) from 1^{st} January 2005 to 1^{st} January 2020. Data from Yahoo Finance.

VIX derivatives pricing formulas:

$$VIX_T^2 := \mathbb{E}\left[\frac{1}{\Delta}\int_T^{T+\Delta} \frac{d < S, S >_t}{S_t^2} | \mathcal{F}_0\right], \tag{0.0.2}$$

$$\text{VIX Futures,} \quad V_t^T := \mathbb{E}\left[VIX_T | \mathcal{F}_t\right], \tag{0.0.3}$$

$$\text{VIX Options,} \quad C(VIX_0, K, T) := \mathbb{E}\left[(VIX_T - K)^+ | \mathcal{F}_0\right] = \mathbb{E}\left[(V_t^T - K)^+ | \mathcal{F}_0\right], \tag{0.0.4}$$

with K the strike price and Δ one month.

Figure (1) clearly shows that the VIX index reflects the volatility of SPX. Hence, the values of options on SPX and options on VIX should be somehow related. Although VIX options are among the most liquid financial derivatives in the world because they provide market participants another tool to manage volatility, the bid-ask spreads in the VIX options market demonstrate that financial institutions do not have a reliable pricing methodology for these products. Taking into account that SPX and VIX are closely related to each other, any methodology designed to price VIX options must be consistent with the pricing of SPX options. This suggests that researchers must develop a model capable of jointly calibrating SPX and VIX option prices. It is the joint S&P 500/VIX smile calibration problem.

This issue was briefly tackled thanks to jump models which have been proposed by Carr and Madan in [6] and by Kokholm and Stisen in [7]. Nevertheless, those models do not really achieve a satisfying accuracy for the joint calibration problem. Regarding this challenge, Julien Guyon stated that "joint calibration seems out of the reach of continuous time models with continuous SPX paths". However, Jim Gatheral et al. found a counterexample to Guyon's conjecture in [8].

The purpose of this paper is to introduce readers to the emerging class of rough volatility models and their possible applications to the pricing of VIX and SPX options.

The paper is structured as follows. Throughout the first chapter, we focus on the reasons that motivate practitioners and researchers to consider rough volatility models. It focuses on the properties of the historical time series of volatility. This chapter shows that the logarithm of volatility behaves essentially as a fractional Brownian motion with Hurst exponent H of order 0.1, unlike what stated Comte and Renault in [3]. Finally, given the observations made in the first

chapter, chapter 2 tackles calibration with option implied volatility surface within three rough volatility models: the rough Bergomi model, the rough Heston model and the quadratic rough Heston model. All the calibrations are performed over real market data from Yahoo Finance.

Chapter 1

Motivations

The rough nature of the volatility time series is now widely accepted within Equity markets. It has been first discovered by Gatheral, Jaisson and Rosenbaum in [1] and then confirmed by Mathieu Rosenbaum et al. in [9] and by Fukasawa in [10].

The objective of this first chapter is to understand how those authors shew that the volatility time series presents a rougher trait than that of a Brownian motion.

1.1 Motivation I: The implied volatility surface

Recall that the implied volatility of an option is the value of the volatility parameter required in the model we considered, to match the observed market price of that same option. Plotting the implied volatility depending on the time to maturity and the strike price of the option gives the implied volatility surface.

We first shed lights on the limits of the Black-Scholes model with respect to the implied volatility surface. Consider a given probability space $(\Omega, \mathcal{F}, \mathbb{P})$ with a Brownian motion $(W_t)_{t\geq 0}$. In the Black-Scholes model, the stock price process $(S_t)_{t\geq 0}$ has the following dynamics

$$\frac{\mathrm{d}S_t}{S_t} = r\mathrm{d}t + \sigma \mathrm{d}W_t, \qquad S_0 > 0, \tag{1.1.1}$$

where r and $\sigma > 0$ denote respectively the instantaneous risk-free rate and the spot volatility. Note that σ is constant and deterministic and it is also the only unknown parameter of the model. Therefore, if this model is completely correct, the implied volatility surface across strike price and time to maturity should be flat. But Figure (1.1) clearly shows that the implied volatility surface is not flat. Hence, the BS model does not give a correct approach of the volatility.

Note that Figure (1.1) displays the implied volatility derived by using the Newton's method, which is a root finding algorithm. Nevertheless, it could have been possible to use data provided by the CBOE website as well. Figure (1.2) compares both implied volatility smiles. One can note that both curves look similar.

Still about the Figure (1.1), it can be considered as stylized fact that the overall shape of the volatility surface in Equity markets does not change over time, at least to a first approximation. This observation suggests to consider volatility as a time homogeneous process, *i.e.* a process whose parameters are independent of price and time.

However, even conventional time homogeneous model that consider the volatility as a stochastic process (such as the Hull and White, Heston, and SABR models) also fail to properly fit the volatility surface, in particular the at-the-money (when the strike price K equals the spot price) volatility skew which is defined by

$$\psi(\tau) := \left| \frac{\partial \sigma(K,\tau)}{\partial K} \right|_{K=S_t} \tag{1.1.2}$$

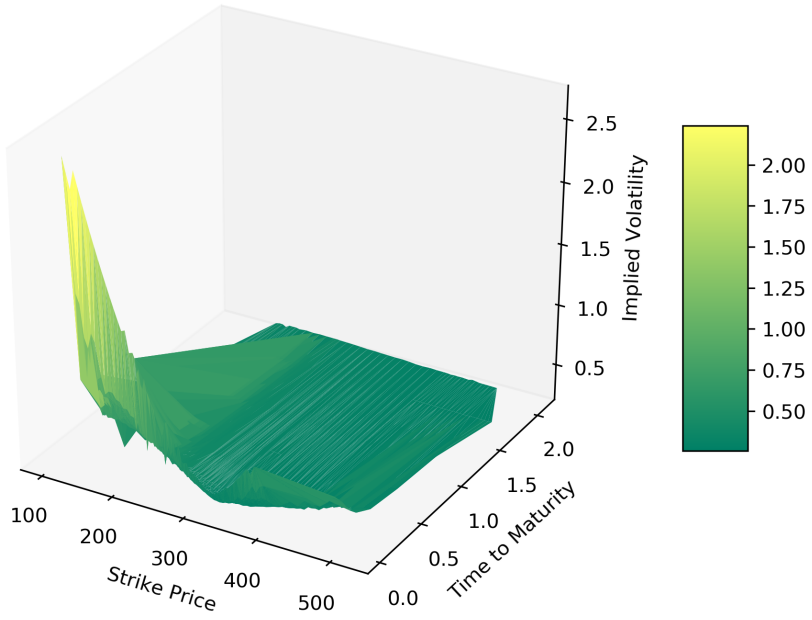

Figure 1.1: The AAPL Call options volatility surface as of May 18, 2020. Implied volatility derived by using the Newton's method.

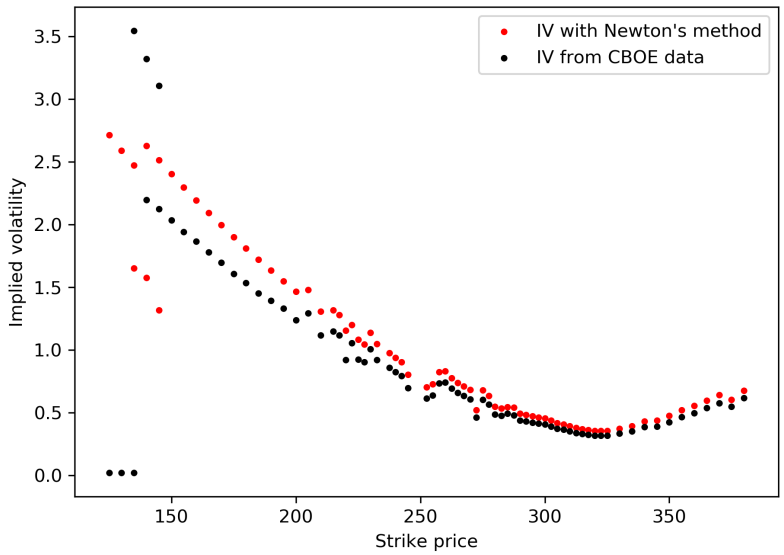

Figure 1.2: Comparison between the derived implied volatility (with Newton's method) and the implied volatility given by CBOE.

To plot the ATM volatility skew, the latter derivative was approximated by the following expression

$$\psi(\tau) \approx \left| \frac{\sigma(S_t + \epsilon, \tau) - \sigma(S_t - \epsilon, \tau)}{2\epsilon} \right|, \tag{1.1.3}$$

for ϵ small.

Existing time-independent stochastic volatility models generate ATM volatility skew constant for short dates and inversely proportional to τ for long dates in contrast to the ATM skew observed in the market, see Figure (1.3), that behaves as a power law of the form $\psi(\tau) = A\tau^{-0.4}$.

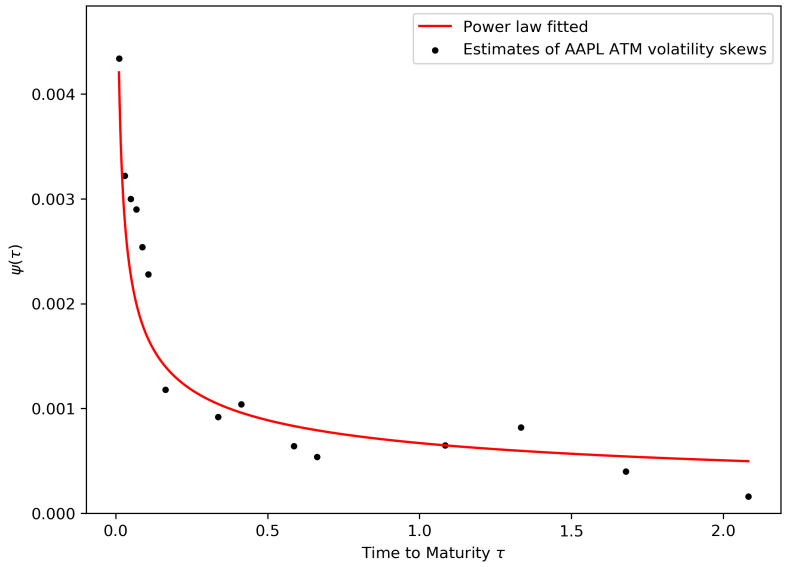

Figure 1.3: Estimates of the AAPL volatility skews as of May 18 2020 with the fitted power-law $\psi(\tau) = A\tau^{-0.4}$.

Nonetheless, in [5, Section 3.3], Fukasawa demonstrates that a stochastic volatility model where the volatility is driven by a fractional Brownian motion with Hurst index H leads to an ATM volatility skew of the form $\psi(\tau) \sim \tau^{H-\frac{1}{2}}$. Hence, for such a model, in order to be consistent with the shape of the implied volatility surface, $H < 1/2$ is required. This yields in losing the long memory property, widely accepted as a stylized fact, that motivated Comte and Renault to use the fractional Brownian motion to model log-volatility.

Following this observation, Gatheral, Jaisson and Rosenbaum in [1] went further in the study of the volatility time series modeling by focusing on its stylized facts.

1.2 Motivation II: Properties of the historical time series of volatility

The procedure described in this section is mainly inspired by [1].

Throughout this section, since the spot variance is not directly observable in the market, daily estimates of the realized variance from the Oxford-Man Institute are used as proxies instead.

1.2.1 Estimating the smoothness of the volatility process

In order to measure the roughness of the historical volatility time series, we look at the the q^{th} sample moment of log volatility increments at a given lag Δ defined by

$$m(q, \Delta) := \frac{1}{N} \sum_{k=1}^{N} \left| log(\sigma_{k\Delta}) - log(\sigma_{(k-1)\Delta}) \right|^q, \tag{1.2.1}$$

where $\sigma_\Delta, ..., \sigma_{N\Delta}$ are observations of the volatility process on a time grid with mesh Δ on $[0, T]$ with $N = \lfloor T/\Delta \rfloor$. Note that $m(2, \Delta)$ is just the sample variance of the difference in log volatility at the lag Δ. Moreover, we assume there exists $s_q > 0$ and $b_q > 0$ such that

$$m(q, \Delta) \underset{\Delta \to 0}{\sim} b_q N^{-qS_q}. \tag{1.2.2}$$

Although realized variance estimates are used as proxies of the instantaneous volatility, they make it possible to derive and plot $m(q, \Delta)$ vs $log(\Delta)$, see Figure (1.4) for the S&P index.

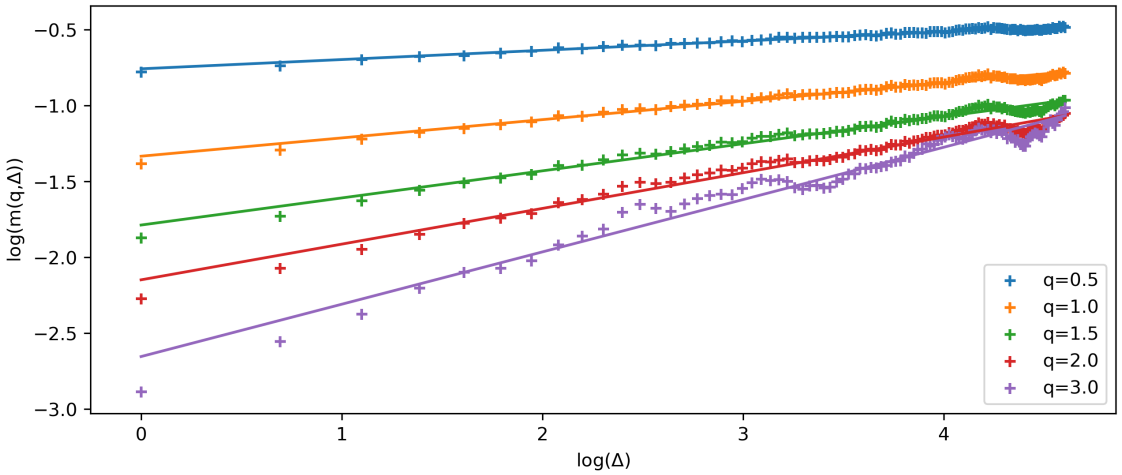

Figure 1.4: $log(m(q, \Delta))$ as a function of $log(\Delta)$, S&P 500 index.

One can easily note that for a given value of q, the points of $m(q, \Delta)$ lies on a straight line. Hence, a linear regression yields the following result

$$log(m(q, \Delta)) = \zeta_q log(\Delta) + B_q \iff m(q, \Delta) = \Delta^{\zeta_q} e^{B_q}, \tag{1.2.3}$$

where ζ_q and B_q are two constants depending on q. Furthermore, by considering that the increments of the log-volatility are independent and stationary, *i.e.* $log(\sigma_{k\Delta}) - log(\sigma_{(k-1)\Delta}) \sim log(\sigma_\Delta)$ in distribution, the Strong Law of Large Numbers gives the following convergence almost surely

$$m(q, \Delta) \underset{N \to \infty}{\to} \mathbb{E}\left[|log(\sigma_\Delta) - log(\sigma_0)|^q\right]. \tag{1.2.4}$$

Finally we have

$$\mathbb{E}\left[|log(\sigma_\Delta) - log(\sigma_0)|^q\right] = \Delta^{\zeta_q} e^{B_q}. \tag{1.2.5}$$

And plotting ζ_q against q shows that $\zeta_q \sim Hq$ with $H \approx 0.1133$ for S&P, see Figure (1.5). H denotes the smoothness of the volatility.

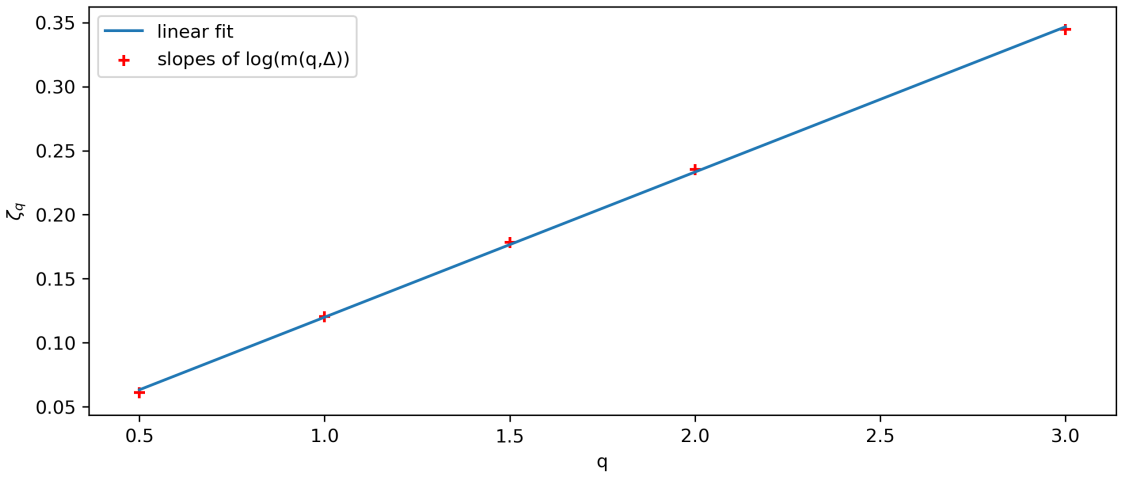

Figure 1.5: ζ_q (in red) and $\zeta_q \sim Hq$ (in blue), S&P.

1.2.2 Other indices

The study on every other index in the Oxford-Man Institute dataset leads to a universal scaling behavior of $m(q, \Delta)$. By repeating the exact same process on each index with $q \in \{0.5, 1, 1.5, 2, 3\}$, we obtain the estimates of H given in Table (A.1), see Appendix (A.1). From the latter table, we conclude that $H \approx 0.1$.

1.2.3 Distribution of the increments of the log-volatility

Andersen and al. demonstrated in [11] that the distribution of increments of log-volatility is close to a Gaussian distribution. Figure (1.6) displays the histograms of the increments of the log-volatility with the fitted normal density superimposed in red for the S&P index. It is clear that with the latter figure, we retrieve the stylized fact stated in [11]. Added to the plots is the 1-day fit of the normal density rescaling by Δ^H (blue dashed curves). Note that these are very close to the red fits of the normal density.

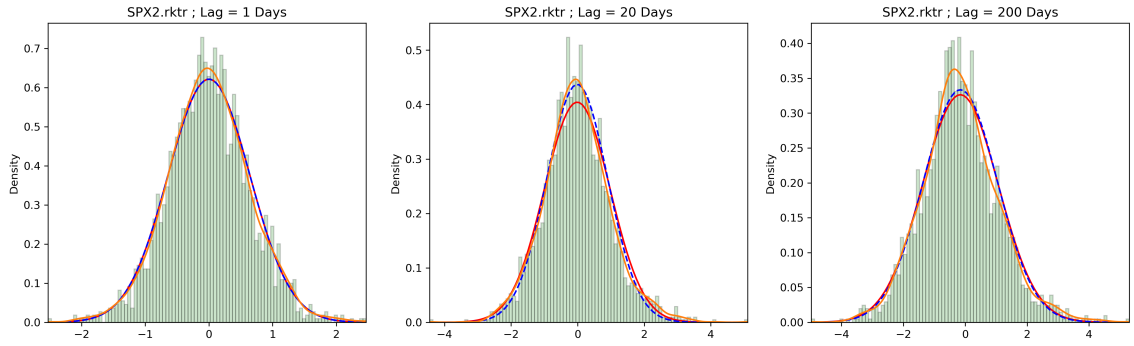

Figure 1.6: Histograms of the increments $(log(\sigma_{t+\Delta}) - log(\sigma_t))$ for various lags Δ of the S&P log-volatility.

1.2.4 Does H vary over the time ?

Is the smoothness parameter H constant over the time ? In order to answer to that question, we first derived H for each half of the dataset from the Oxford-Man Institute. One can easily note in Table (A.2) that, most of the time, the smoothness parameter is higher in the second period which includes the 2008 financial Crisis.

To get a more precise idea of these variations, we consider the paper [12] which includes the plot in Figure (1.7), of the variation of the estimator $\hat{\alpha} = H - 1/2$ over the time. Several peaks of smoothness seem to coincide with periods of market turmoil. The plot indicates the respective dates of the onset of the subprime mortgage crisis of 2008, the Flash Crash of May 6 2010, the Greek debt crisis in 2011 and finally the Brexit vote.

1.2.5 Elaboration of the model

We shew in the previous section that the distribution of increments of log-volatility is close to Gaussian. This motivates us to model $(\sigma_t)_{t\geq 0}$ as a log-normal random variable. Moreover, the scaling property of variance of RV differences suggests the model:

$$log(\sigma_{t+\Delta}) - log(\sigma_t) = \nu(W^H_{t+\Delta} - W^H_t), \tag{1.2.6}$$

where W^H is a fractional Brownian motion with Hurst index and ν a positive constant. For further information regarding fractional Brownian motion, see Appendix (E.1).

Let us now relate the model described in equation (1.2.6) to the estimates we derived in the

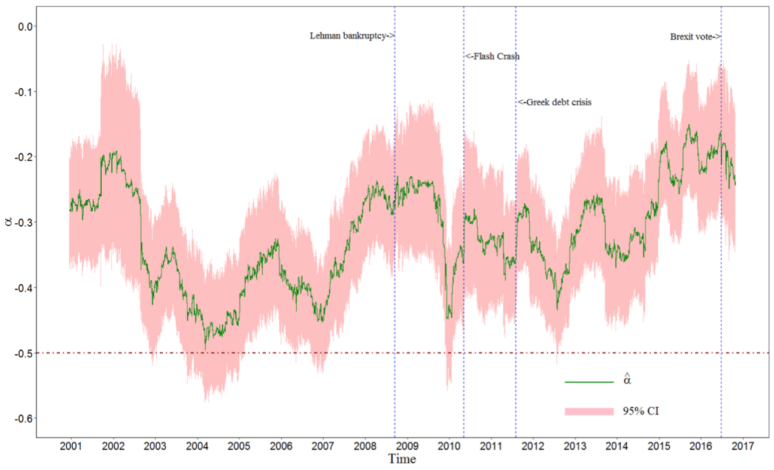

Figure 1.7: Half year rolling-window estimates of α on the realized variance measures of the daily volatility. The pink area is the 95% confidence interval obtained by bootstrap method.

previous sections.

$$\begin{aligned}\mathbb{V}\left[log(\sigma_{t+\Delta}) - log(\sigma_t)\right] &= \mathbb{E}\left[(log(\sigma_{t+\Delta}) - log(\sigma_t))^2\right] = \Delta^{\zeta_2} e^{B_2} \\ &= \Delta^{2H} e^{B_2} = e^{B_2}\left[|t+\Delta-t|^{2H}\right] \\ &= e^{B_2}\mathbb{V}\left[W^H_{t+\Delta} - W^H_t\right] \\ &= \mathbb{V}\left[e^{B_2/2}(W^H_{t+\Delta} - W^H_t)\right].\end{aligned}$$

Finally, we observe that the Hurst parameter is equal to the measured smoothness of the volatility and that the constant ν satisfies the following equality: $\nu = e^{B_2/2}$. From the equation (1.2.6), we could deduce the following expression of the volatility

$$\sigma_t = \sigma e^{\nu W^H_t}, \tag{1.2.7}$$

where σ is another positive constant.

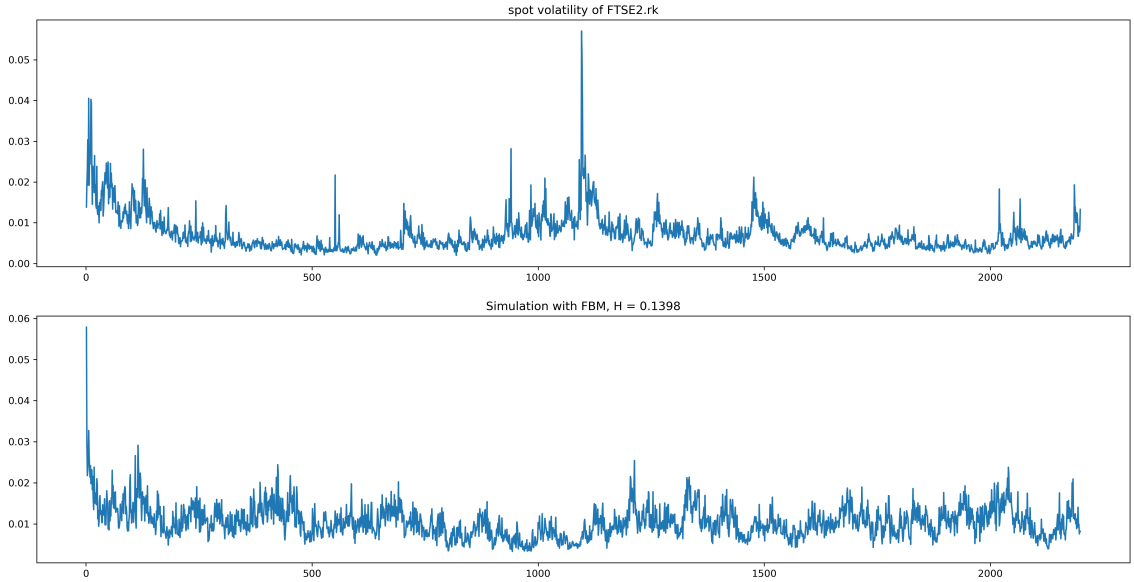

Figure 1.8: Spot Volatility of FTSE Index (above) and in the model described in (1.2.7) with $H = 0.13$ derived empirically (below).

Although that the two plots in Figure (1.8) are not exactly the same, they appear to be as rough as each other. Moreover they both presents persistent periods of low alternate with periods of high volatility with the same order of magnitude.

However, the last model described by equation (1.2.7) does not imply stationary increment, feature very useful for the sake of mathematical tractability. This fact suggests us to consider the log-volatility as a fractional Ornstein-Uhlenbeck (fOU) process with a very long reversion time scale to ensure stationarity.

A stationary fOU process (X_t) is the solution of the stochastic differential equation

$$dX_t = \nu dW_t^H - \alpha(X_t - m)dt, \tag{1.2.8}$$

with $m \in \mathbb{R}$ and α and ν two positive constants. There exists an explicit closed-form formula of the solution of (1.2.8) given by

$$X_t = \nu \int_{-\infty}^{t} e^{-\alpha(t-s)} dW_t^H + m. \tag{1.2.9}$$

Finally, our rough fractional stochastic volatility model on the time interval $[0, T]$ becomes

$$\sigma_t = e^{X_t}, \text{ with } t \in [0, T], \tag{1.2.10}$$

where $(X_t)_{t\in\mathbb{R}}$ satisfies the equation (1.2.9) and $H < 1/2$ the measured smoothness of the volatility. Note that for $\alpha T \ll 1$, the log-volatility behaves locally as a fractional Brownian motion, feature consistent with the observations made.

Jim Gatheral et al. in [1, Section 3.2] shew theoretically that the autocovariance function for the model described in equation (1.2.10) is linear with respect to Δ^{2H}. One can note in Figure (1.9) that this result is satisfied empirically. Indeed, the empirical autocovariance function of the log-volatility is indeed linear with respect to Δ^{2H} for the FTSE Index.

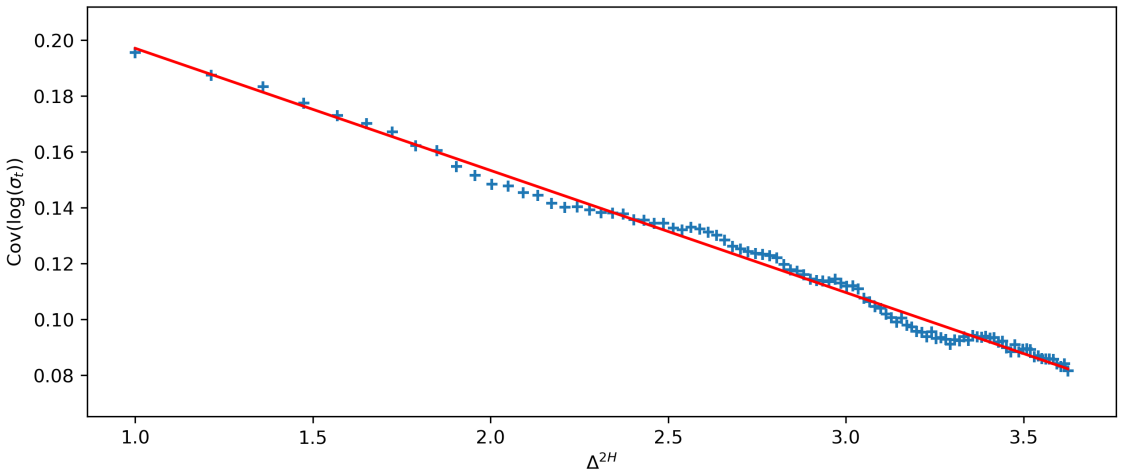

Figure 1.9: Autocovariance of the log-volatility as a function of Δ^{2H} , FTSE Index.

1.2.6 $H < 1/2$ or $H > 1/2$?

The fractional stochastic volatility model is said to be rough if $H < 1/2$. However Comte & Renault used to consider $H > 1/2$ in the model (1.2.10) so as to ensure long memory property, *i.e* the autocorrelation function is not integrable and it decays slowly as a power-law with exponent less than 1. Nevertheless, we first saw, thanks to Fukasawa's work, in [5, Section 3.3], that $H > 1/2$ conducts to an increasing volatility skew with respect to the time to maturity, which is completely inconsistent with the observations made, see Figure (1.3). Hence Comte & Renault are forced to take $\alpha T \ll 1$ to generate a decreasing term structure of volatility skew for longer expirations in the model described in (1.2.10). But for very short expirations ($\tau \ll 1/\alpha$) this implies a term structure of volatility skew that is inconsistent with the observed one.

Nonetheless choosing $H < 1/2$ allows us to reproduce both the observed smoothness of the volatility process, see Figure (1.8), and generate a consistent volatility skew with observed volatility data under the physical measure $\mathbb{P}$. Moreover, taking $H < 1/2$ ensures mean reversion: if the volatility is unusually high, it tends to decline. The opposite is true as well.

Furthermore, the model (1.2.10) allows us to demonstrate the incompatibility of the long memory property, *i.e* $H > 1/2$, with real market data. Indeed, with Figure (1.10), one can note that for small lags, the slope of the regression line is driven by H. Afterwards, the curve begins to flatten at a time scale of order $1/\alpha$. Hence to fit to market data, we must take H equal the slope of the yellow regression line ($H \approx 0.14$, see Appendix (A.1)) and α small enough to prevent the curve from flattening. Thanks to [1, Section 3.2], we had the following formulas to plot the curves in Figure (1.10):

$$\begin{aligned} m(2,\Delta) &= \mathbb{E}\left[\left(log(\sigma_{t+\Delta}) - log(\sigma_t)\right)^2\right], \\ &= 2\left(Var(log(\sigma_t)) - Cov\left[log(\sigma_t), log(\sigma_{t+\Delta})\right]\right), \end{aligned}$$

with

$$Var(log(\sigma_t)) = \frac{H(2H-1)\nu^2}{\alpha^{2H}}\Gamma(2H-1), \tag{1.2.11}$$

and

$$Cov\left[log(\sigma_t), log(\sigma_{t+\Delta})\right] = \frac{H(2H-1)\nu^2}{2\alpha^{2H}}\left(e^{-\alpha\Delta}\Gamma(2H-1) + e^{-\alpha\Delta}\int_0^{\alpha\Delta}\frac{e^u}{u^{2-2H}}du + e^{\alpha\Delta}\int_{\alpha\Delta}^{\infty}\frac{e^{-u}}{u^{2-2H}}du\right). \tag{1.2.12}$$

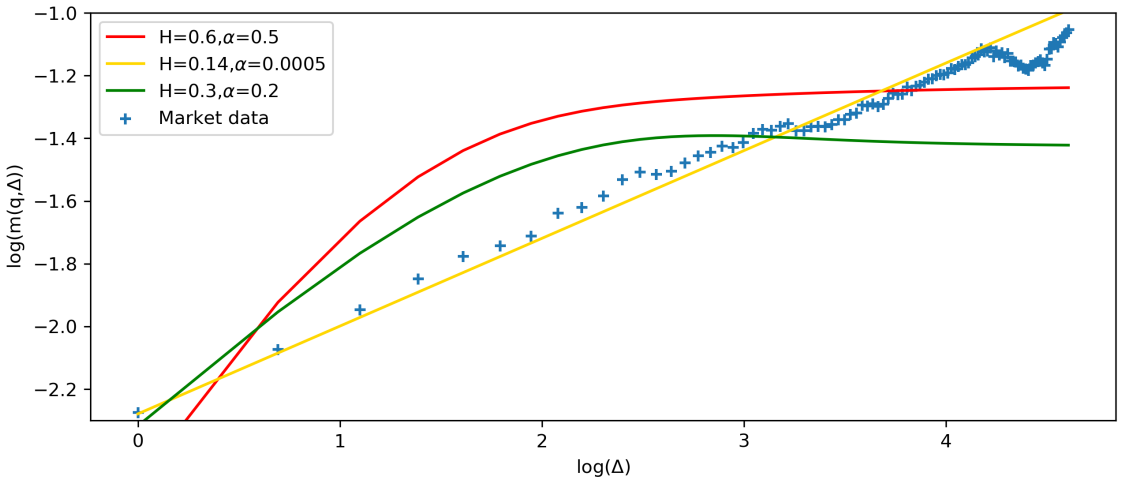

Figure 1.10: Blue crosses are empirical estimates of $m(2,\Delta)$ from historical data of S&P 500 Index. The three other curves are obtained from the model (1.2.10).

Hence, we have shown that the log-volatility process behaves essentially as a fractional Brownian motion with Hurst exponent H of order 0.1 . Such model is remarkably consistent with historical data since it reproduces all the main stylised facts of historical volatility time series and it provides promising fits to implied volatility surfaces, see Figure (1.3).

Chapter 2

Stochastic Volatility Models

We previously shed light on the rough nature of the spot log-volatility. We shew that the latter process behaves as a fractional Brownian motion with Hurst index $H < 1/2$. Such dynamics of the log-volatility reproduces the properties of the historical time series of the volatility and provide a good fit to implied volatility surface as well.

From now, we focus on rough stochastic volatility models for derivatives pricing. Our objective is to implement and calibrate those rough volatility models with real market data. Finally, we will test them to see whether or not they can calibrate jointly SPX and VIX implied volatility smiles.

2.1 The Rough Bergomi Model

2.1.1 Pricing under the physical measure $\mathbb{P}$

Following the previous chapter, we concluded that the logarithm of realized variance, denoted by $(v_t)_{t\geqslant 0}$ (used as proxy for the instantaneous variance), of the underlying price process behaves essentially as a fractional Brownian motion, with Hurst index H. Hence this yields the following the model

$$log(v_{t+\Delta}) - log(v_t) = 2\nu(W^H_{t+\Delta} - W^H_t), \tag{2.1.1}$$

with W^H a fractional Brownian motion and H the Hurst index.

Let us now consider the Mandelbrot-Van Ness representation of fractional Brownian motion W^H in terms of Wiener integrals (see also in Appendix (E.1)) given by

$$W^H_t = C_H \left\{ \int_{-\infty}^t \frac{dW^{\mathbb{P}}_s}{(t-s)^\gamma} - \int_{-\infty}^0 \frac{dW^{\mathbb{P}}_s}{(-s)^\gamma} \right\}, \tag{2.1.2}$$

with $\gamma = 1/2 - H$ and $C_H = \sqrt{\frac{2H\Gamma(3/2-H)}{\Gamma(H+1/2)\Gamma(2-2H)}}$.

The equation (2.1.1) applied to the time $u > t > 0$ with the Mandelbrot-Van Ness representation gives

$$\begin{aligned} log(v_u) - log(v_t) &= 2\nu C_H \left(\int_{-\infty}^u \frac{dW^{\mathbb{P}}_s}{(u-s)^\gamma} - \int_{-\infty}^t \frac{dW^{\mathbb{P}}_s}{(t-s)^\gamma} \right), \\ &= 2\nu C_H \left(\int_t^u \frac{dW^{\mathbb{P}}_s}{(u-s)^\gamma} + \int_{-\infty}^t \left[\frac{1}{(u-s)^\gamma} - \frac{1}{(t-s)^\gamma} \right] dW^{\mathbb{P}}_s \right), \\ &=: 2\nu C_H \left(M_t(u) + Z_t(u) \right), \end{aligned} \tag{2.1.3}$$

where $M_t(u)$ is a Gaussian centred distribution independent of $\mathcal{F}_t$ and $Z_t(u)$ is adapted to the filtration $(\mathcal{F}_t)_{t\geqslant 0}$.

Furthermore, we introduce $\tilde{W}^{\mathbb{P}}_t(u) := \sqrt{2H} \int_t^u \frac{dW^{\mathbb{P}}_s}{(u-s)^\gamma}$, a Volterra fractional Brownian motion, and the deterministic parameter $\eta := 2\nu C_H / \sqrt{2H}$.

Definition 2.1.1 (Volterra process, definition from [13])**.** A Volterra process is given by

$$M(t) = \int_0^t F(t,s)dX_s, \tag{2.1.4}$$

with $(X_t)_{t\geq 0}$ a semimartingale and F a bounded deterministic real-valued function of two variables which sometimes is called a kernel.

Remark 2.1.2. $\tilde{W}^{\mathbb{P}}$ is said to be a Volterra fractional Brownian motion since the kernel function is of the form $F(t,s) = (t-s)^{-\gamma}$ with $\gamma \in [0, 1/2]$, similar to the kernel function found in the Mandelbrot-Van Ness representation of the fractional Brownian motion, see Appendix (E.1).

So finally, (2.1.3) becomes:

$$v_u = v_t exp\left\{\eta\tilde{W}_t^{\mathbb{P}}(u) + 2\nu C_H Z_t(u)\right\}. \tag{2.1.5}$$

Since $\mathbb{E}^{\mathbb{P}}[v_u|\mathcal{F}_t] = v_t exp\left\{2\nu C_H Z_t(u) + 1/2\eta^2\mathbb{E}|\tilde{W}_t^{\mathbb{P}}(u)|^2\right\}$, one can note that the instantaneous variance can be written as

$$v_u = \mathbb{E}^{\mathbb{P}}[v_u|\mathcal{F}_t]\,\mathcal{E}\left(\eta\tilde{W}_t^{\mathbb{P}}(u)\right), \tag{2.1.6}$$

with $\mathcal{E}$ the (Wick) stochastic exponential, given by $\mathcal{E}(\Psi) = exp\left(\Psi - 1/2\mathbb{E}^{\mathbb{P}}|\Psi|^2\right)$. The equation (2.1.6) highlights that the distribution of v_u depends on $\mathcal{F}_t$ only through the forward variance curve, $\mathbb{E}^{\mathbb{P}}[v_u|\mathcal{F}_t]$, also denoted by $\xi_t(u)$. Therefore, if somehow we can observe the forward variance curve in the market, it is giving us all the information about the history of the Brownian motion that we need to be able to compute the price of the options.

2.1.2 Pricing under $\mathbb{Q}$

In order to price under $\mathbb{Q}$, we need to do a change of measure. In general a change of measure could depend on anything. In our case, we consider a change of measure of the form

$$dW_s^{\mathbb{P}} = dW_s^{\mathbb{Q}} + \lambda(s)ds, \tag{2.1.7}$$

where $\lambda(s)$ is deterministic and can be interpreted as the price of volatility risk.
Some algebras give

$$\begin{aligned} v_u &= \mathbb{E}^{\mathbb{P}}[v_u|\mathcal{F}_t]\,\mathcal{E}\left(\eta\tilde{W}_t^{\mathbb{Q}}(u)\right) exp\left\{\eta\sqrt{2H}\int_t^u \frac{\lambda(s)}{(u-s)^\gamma}ds\right\}, \\ &= \xi_t(u)\mathcal{E}\left(\eta\tilde{W}_t^{\mathbb{Q}}(u)\right), \\ &= \xi_t(u)exp\left\{\eta\tilde{W}_t^{\mathbb{Q}}(u) - \frac{1}{2}\eta^2u^{2H}\right\}, \end{aligned} \tag{2.1.8}$$

with, by definition,

$$\xi_t(u) = \mathbb{E}^{\mathbb{Q}}[v_u|\mathcal{F}_t] = \mathbb{E}^{\mathbb{P}}[v_u|\mathcal{F}_t]\,exp\left\{\eta\sqrt{2H}\int_t^u \frac{\lambda(s)}{(u-s)^\gamma}ds\right\}. \tag{2.1.9}$$

The latter equation defines the so-called forward variance curve. One can note that the equation (2.1.8) is actually a non-Markovian generalization of the Bergomi model, also called rough Bergomi model.

2.1.3 Specifications of the rough Bergomi model

Following the deterministic change of measure written in the previous section, the model turns out to be a non-Markovian extension of the well-known Bergomi model, which we called the Rough Bergomi model. This model, under the pricing measure $\mathbb{Q}$, is given by

$$\begin{cases} dS_t &= S_t\sqrt{v_t}dZ_t, \\ dZ_t &= \rho dW_t + \sqrt{1-\rho^2}dW_t^\perp, \\ v_u &= \xi_0(u)\mathcal{E}\left(\eta\sqrt{2H}\int_0^u \frac{1}{(u-s)^\gamma}dW_s\right) = \xi_0(u)\mathcal{E}\left(\eta\tilde{W}_u\right), \\ \xi_t(u) &= \mathbb{E}^{\mathbb{P}}[v_u|\mathcal{F}_t]\,exp\left(\eta\sqrt{2H}\int_t^u \frac{\lambda(s)}{(u-s)^\gamma}ds\right). \end{cases} \tag{2.1.10}$$

with W and $W^{\perp}$ two independent Brownian motion. S and v denote respectively the price and the spot variance process of the underlying. ρ is the correlation between volatility moves and price moves. $\tilde{W}$ is a Volterra process that satisfies for any $v > u > 0$:

$$\begin{cases} cov\left[\tilde{W}_u \tilde{W}_v\right] & = u^{2H} G(\frac{u}{v}), \\ Var\left[\tilde{W}_u\right] & = u^{2H}, \end{cases} \tag{2.1.11}$$

where

$$G(x) = \frac{1-2\gamma}{1-\gamma} x^{\gamma} {}_2F_1(1, \gamma, 2-\gamma, x), \tag{2.1.12}$$

with ${}_2F_1$ the confluent hypergeometric function. As mentioned above, this rough Bergomi model is non-Markovian in the instantaneous variance v_t since $\mathbb{E}^{\mathbb{Q}}[v_u|\mathcal{F}_t] \neq \mathbb{E}^{\mathbb{Q}}[v_u|v_t]$.

Unlike in the conventional Bergomi model, there is no exponential kernel in the exponent of the forward variance curve given in (2.1.10). Note that the latter is replaced by a power-law kernel which generates a volatility skew of the form $\psi(\tau) \sim \tau^{-\gamma}$ (see [5, Section 3.3]), this time consistent with the observations from the market. We may therefore expect that the rough Bergomi model will generate a realistic term structure of ATM volatility skew.

2.1.4 Numerical scheme

Considering what it is written in the previous section, it is possible to simulate the rough Bergomi model by using Riemann scheme that relies on the approximation of the kernel function using step functions. However, given that $0 < \gamma < 1/2$, such method fails to capture the explosion of the kernel function near zero within the Volterra process.

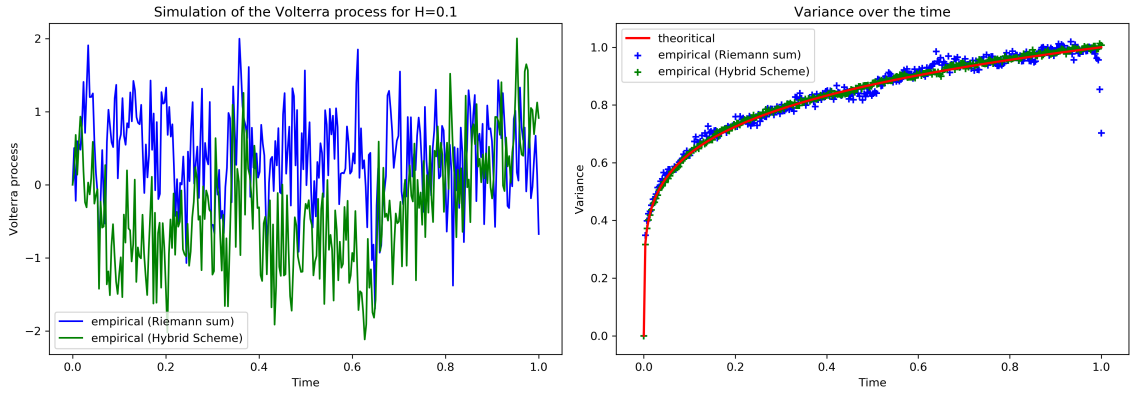

Figure 2.1: Simulation of the Volterra process through the hybrid scheme and the Riemann sum. $H = 0.1$ for both plots.

Hence, the work of Jim Gatheral et al [1] conducts to the quest for efficient pricing method for this model. It is Bennedsen, Lunde and Pakkanen in [4, Section 2.3] who first introduced an hybrid scheme for Brownian semistationay ($\mathcal{BSS}$) processes that enables us to capture the explosion of the kernel function near zero. First, let recall what a $\mathcal{BSS}$ process is:

Definition 2.1.3 (Brownian semistationay process)**.** Let $(\Omega, \mathcal{F}, (\mathcal{F})_{t\in\mathbb{R}}, \mathbb{P})$ be a filtered probability space, satisfying the usual conditions, supporting a (two-sided) standard Brownian motion W. We consider a Brownian semistationary process

$$X(t) := \int_{-\infty}^{t} g(t-s)\sigma(s)dW_s, \quad t \in \mathbb{R}. \tag{2.1.13}$$

where σ is an $\{\mathcal{F}_t\}_{t\in\mathbb{R}}$-predictable process with locally bounded trajectories, and g is a positive Borel measurable kernel function. To make sure that the integral (2.1.13) is finite, we assume that

the kernel function g is square integrable, so $\int_0^\infty g(x)^2 dx < \infty$. Futher assumptions are needed to develop this scheme, see [4, Section 2].

Within the hybrid scheme, the kernel function is approached by a power function near zero and by a step function elsewhere. The resulting approximation of the process is a combination of Wiener integrals of the power function and a Riemann sum, hence hybrid scheme. This scheme is only slightly more demanding to implement than the Riemann sum scheme and the schemes have the same computational complexity as the number of discretization cells tends to infinity. Furthermore, one can note in Figure (2.1) that the hybrid scheme outputs very close results to the theoritical ones. Switching from the Riemann sum to the hybrid scheme reduces the asymptotic root mean square error as well, see [4, Section 2.4].

Definition 2.1.4 (Hybrid scheme)**.** As explained in [4, Section 2.3], the hybrid scheme applied to the $\mathcal{BSS}$ process in (2.1.13) gives

$$X(t) = \sum_{k=1}^{\infty} \int_{t-k/n}^{t-k/n+1/n} g(t-s)\sigma(s)dW_s \approx \sum_{k=1}^{\infty} \sigma(t-\frac{k}{n}) \int_{t-k/n}^{t-k/n+1/n} g(t-s)dW_s. \tag{2.1.14}$$

if k is small, we consider

$$g(t-s) \approx (t-s)^\alpha L_g\left(\frac{k}{n}\right), \quad (t-s) \in \left[\frac{k-1}{n}, \frac{k}{n}\right] \setminus \{0\}, \tag{2.1.15}$$

with L_g that varies less than the power function $y \mapsto y^\alpha$ near zero. Otherwise, if k is large, or at least $k \geq 2$, then taking $b_k \in [k-1, k]$ provides an adequate approximation

$$g(t-s) \approx g\left(\frac{b_k}{n}\right), \quad (t-s) \in \left[\frac{k-1}{n}, \frac{k}{n}\right]. \tag{2.1.16}$$

So finally, (2.1.14) becomes

$$X(t) \approx \sum_{k=1}^{\kappa} L_g\left(\frac{k}{n}\right) \sigma(t-\frac{k}{n}) \int_{t-k/n}^{t-k/n+1/n} (t-s)^\alpha dW_s + \sum_{k=\kappa+1}^{\infty} g\left(\frac{b_k}{n}\right) \sigma(t-\frac{k}{n}) \int_{t-k/n}^{t-k/n+1/n} dW_s. \tag{2.1.17}$$

From now, the hybrid scheme is used to simulate the Volterra process instead of the Riemann sum method. To simulate the Volterra process $\tilde{W}_t := \sqrt{2H}\int_0^t (t-s)^\alpha dW_s$ with $\gamma = -\alpha$ to stay consistent with the previous notations, we implemented the first-order variant ($\kappa = 1$) of the hybrid scheme given by

$$\tilde{W}_{t_i} \approx \sqrt{2H}\left(\int_{\frac{i-1}{n}}^{\frac{i}{n}} \left(\frac{i}{n} - s\right)^\alpha dW_s + \sum_{k=2}^{i} \left(\frac{b_k}{n}\right)^\alpha \left(W_{\frac{i-(k-1)}{n}} - W_{\frac{i-k}{n}}\right)\right), \tag{2.1.18}$$

with

$$b_k := \left(\frac{k^{\alpha+1} - (k-1)^{\alpha+1}}{\alpha+1}\right)^{\frac{1}{\alpha}}. \tag{2.1.19}$$

The latter discretization (b_k) is the one that minimizes the asymptotic mean square root, see [4, Proposition 2.8].

Once the price process $(S_t^i)_{t>0, 1\leq i\leq M}$ is simulated within the rough Bergomi model by using $S_t = S_0 exp\left\{\int_0^t \sqrt{v_u} dZ_u - \frac{1}{2}\int_0^t v_u du\right\}$, we introduce implied volatility estimators

$$\hat{\sigma}_{BS}^M(k,t) = BS^{-1}\left(\hat{C}_M(k,t)\right), \tag{2.1.20}$$

with

$$\hat{C}_M(k,t) = \frac{1}{M}\sum_{i=1}^{M} \left(S_t^i - e^k\right)^+ \approx \mathbb{E}\left[(S_t - K)^+\right], \tag{2.1.21}$$

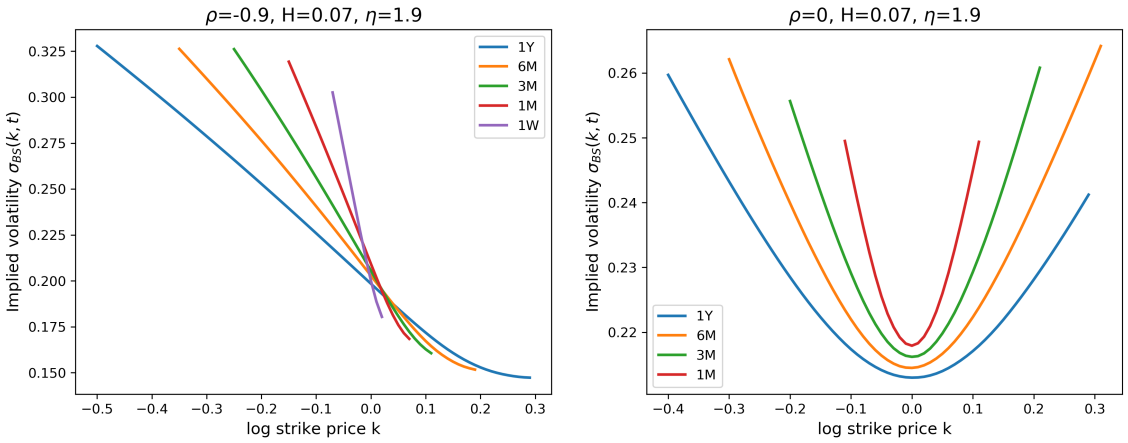

Figure 2.2: Implied volatility smiles simulated by using the hybrid scheme, for maturities going from 1 week to 1 year. The number of paths simulated is 300 000 paths, each over a time interval discretised on a 300-point grid.

where k denotes the log-strike.

Recall that the implied volatility is the right value of σ in Black-Scholes such that the two option prices (the one derived from the rough Bergomi model and the other one from Black-Scholes) are equal.

The latter method makes it possible to study the impact of the three time-homogeneous parameters (H,η,ρ) over implied volatility smiles.

1. H controls the decay of the ATM skew $\psi(\tau)$ for short expirations.

2. η : the product $\rho\eta$ sets the level of the ATM skew for longer expirations.

3. Decreasing ρ pushes the minimum of each smile towards higher strikes.

Then, an intuitive way to rename those paramaters with respect to their influence would be smile for η, skew for ρ and finally roughness for H. Note that the smoothness parameter H and η stay unchanged under $\mathbb{P}$ and $\mathbb{Q}$. Moreover both of them can be estimated from historical data.

Figures (2.2) and (2.3) show implied volatility smiles obtained within the rough Bergomi model. The values of $\eta = 1.9$ and $\rho = -0.9$ are demonstrated to be consistent with the SPX market on 4 February 2010 in [1, Section 5.3]. Moreover, we assumed throughout the simulation that the forward variance curve is flat, *i.e* $\xi_0(u) = \xi$. The two figures highlight the influences of the three time-homogeneous parameters mentioned above. Note that the case $H = 0.5$ is similar to classical stochastic volatility models in the absence of time-dependent or randomised parameters, or jump processes.

2.1.5 Fits to one trading day

Implied volatility smiles

In order to examine the performance of the rough Bergomi model, we used SPX historical data from Yahoo Finance website as of June 15, 2020. To fit rough Bergomi smiles with historical market data, we consider the following objective function, which represents the distance between the targeted implied volatilities and the ones from the rough Bergomi model

$$\sum_k \left(\sigma_k^{Berg}(H,\eta,\rho) - \sigma_k^{Yahoo}\right)^2, \tag{2.1.22}$$

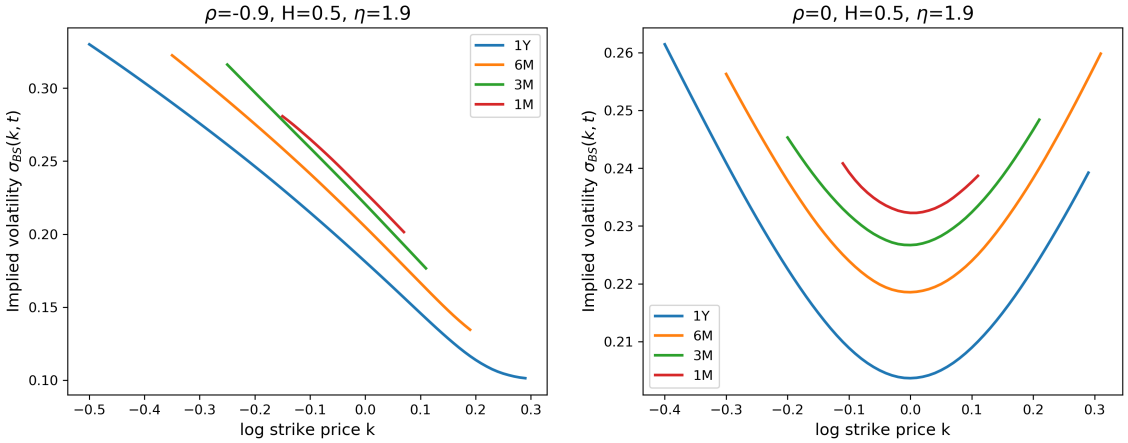

Figure 2.3: Implied volatility smiles simulated by using the hybrid scheme, for maturities going from 1 month to 1 year. The number of paths simulated is 300 000 paths, each over a time interval discretised on a 300-point grid.

subject to the following constraints

$$\begin{cases} H \in (0, 1/2]\,, \\ \eta \geq 0, \\ \rho \in [-1, 1], \end{cases}$$

where $\sigma_k^{Berg}(H, \eta, \rho)$ and σ_k^{Yahoo} are respectively the implied volatilities from the rough Bergomi model and the Yahoo Finance dataset.

With calibrated parameters H, η and ρ, we obtain the plots in Figure (2.4). We took $H \approx 0.11$, obtained from the regression of the second moment of the log-volatility differences, $\eta = 2.3$ and finally $\rho = -0.9$. The plots highlight the impressive fit to the SPX implied volatility smiles.

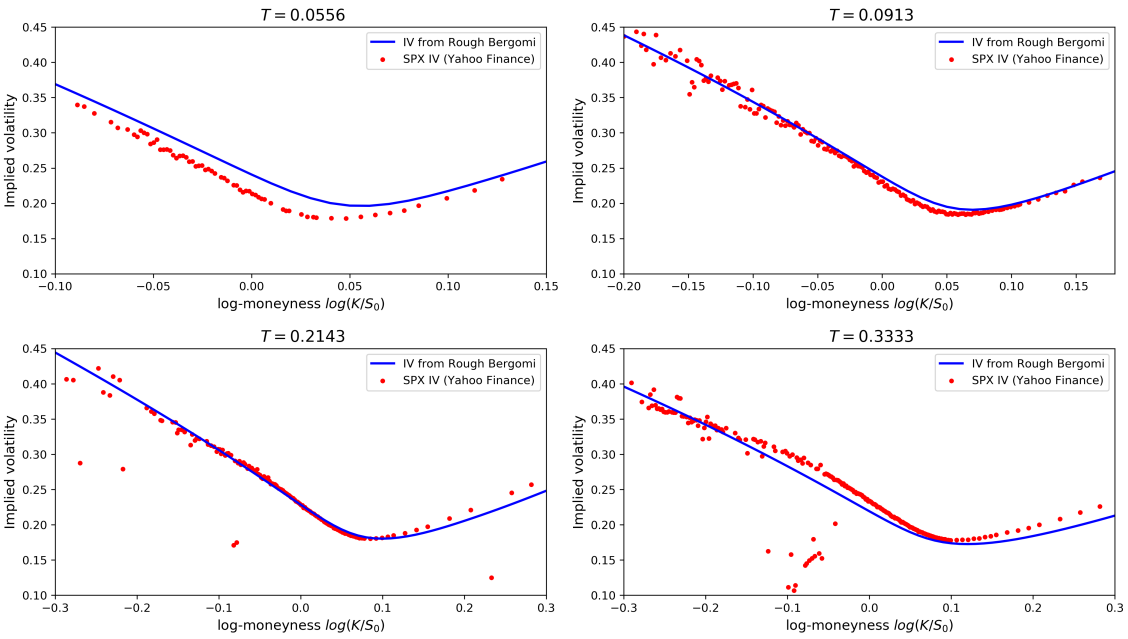

Figure 2.4: Volatility smiles as of July 8, 2020: red dots represent SPX implied volatilities and all the blue lines, coming from the same three parameters, are from the rough Bergomi model. T is time to expiry in years. The IV from the Yahoo finance dataset is actually the mean between the bid and ask implied volatilities.

At-the-money volatility skew

Let us now check whether or not the rough Bergomi model matches with the empirical at-the-money volatility skews obtained from the Yahoo finance dataset. First, recall that the term structure of the at-the-money volatility skew is given by

$$\psi(\tau) := \frac{\partial \sigma_{iv}(K,\tau)}{\partial K}\bigg|_{K=S_t}, \tag{2.1.23}$$

where K is the strike price. Since the dataset does not include any at-the-money volatility skew, the finite difference method was used to estimate it. So, for ϵ small, we have

$$\psi(\tau) := \frac{\partial \sigma_{iv}(K,\tau)}{\partial K}\bigg|_{K=S_t} \approx \frac{\sigma_{iv}(S_t+\epsilon,\tau) - \sigma_{iv}(S_t-\epsilon,\tau)}{2\epsilon}. \tag{2.1.24}$$

Moreover, thanks the presence of a power-law kernel in the exponent of the forward variance curve, the rough Bergomi model generates a volatility skew of the form $\psi(\tau) \sim \tau^{-\gamma}$. Finally, one can note in Figure (2.5) how well the rough Bergomi fits the ATM volatility skew, as expected.

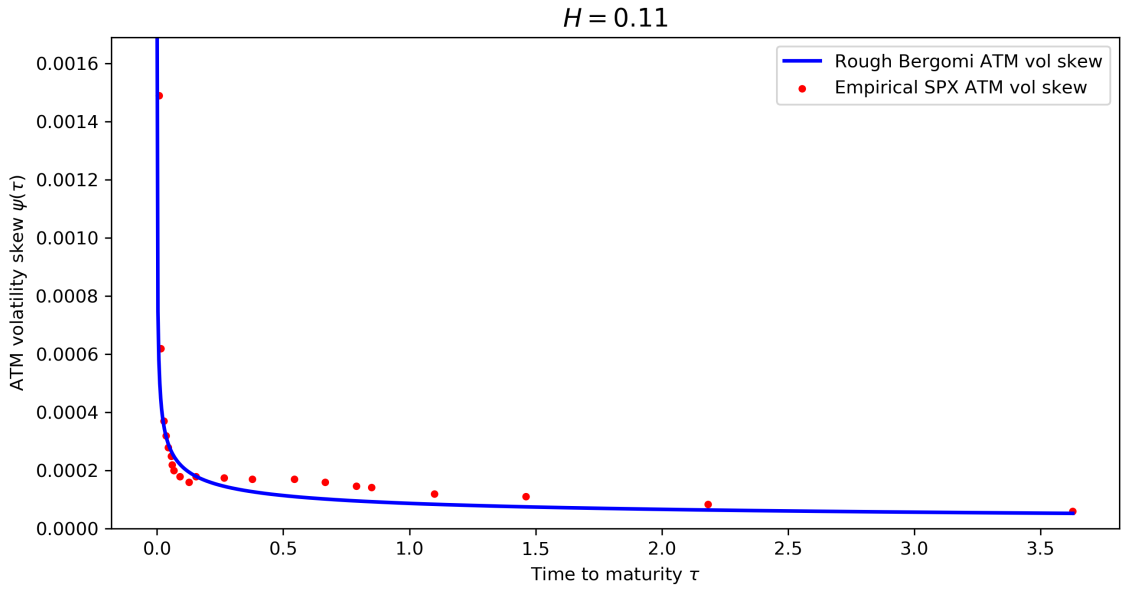

Figure 2.5: ATM Volatility skews as of June 15, 2020: red dots represent empirical SPX ATM volatility skew and the blue line is from the rough Bergomi model. We keep $H \approx 0.11$. τ is time to expiry in years.

2.1.6 The rough Bergomi model and calibration to VIX smiles

Although the rough Bergomi model offers a good fit to the SPX implied volatility surface, it is not consistent with the VIX options market.

Indeed, by using (0.0.2) and the dynamics of the price process S in (2.1.10), we have

$$VIX_T^2 = \mathbb{E}\left[\frac{1}{\Delta}\int_T^{T+\Delta} v_t dt | \mathcal{F}_0\right]. \tag{2.1.25}$$

Hence the latter integral written in the expectation above can be approached with a sum of log-normal distributions (Riemann method) because the instantaneous variance is log-normally distributed in the model, see equation (2.1.8). Therefore we can write

$$VIX_T^2 \approx \mathbb{E}\left[\frac{1}{\Delta}\sum_{i=0}^{N-1} e^{Z_i}\frac{\Delta}{N}\right], \tag{2.1.26}$$

with $(Z_i)_{0\leq i\leq N-1}$ normally distributed. We consider $X_i := e^{Z_i\frac{\Delta}{N}} = e^{\tilde{X}_i}$ where $(\tilde{X}_i)_{0\leq i\leq N-1}$ are independant normal distributions. This notation is acceptable since X_i is log-normal $\forall i \in \{0, ..., N-1\}$. One can note that $(X_i)_{0\leq i\leq N-1}$ is small because of the multiplying factor Δ that represents only one month.

By using the Taylor expansion of the exponential function, we have

$$VIX_T^2 \approx \frac{1}{\Delta}\mathbb{E}\left[N + \sum_{i=0}^{N-1}\tilde{X}_i\right] = \frac{1}{\Delta}\mathbb{E}\left[N - 1 + exp\left\{\sum_{i=0}^{N-1}\tilde{X}_i\right\}\right], \tag{2.1.27}$$

Finally, taking the square root of (2.1.27) combined with the Taylor expansion of the square root function yield

$$VIX_T \approx \sqrt{\frac{N-1}{\Delta}}\left(1 + \frac{1}{2(N-1)}\mathbb{E}\left[exp\left\{\sum_{i=0}^{N-1}\tilde{X}_i\right\}\right]\right). \tag{2.1.28}$$

Equation (2.1.28) demonstrates that the VIX itself is almost log-normal in the model because $\sum_{i=0}^{N-1}\tilde{X}_i$ is normally distributed.

This generates a flat implied volatility surface, which is not consistent with the market observations, see Figure (2.6) that exhibits a pronounced positive skew. Finally, the rough Bergomi model fits accurately index option smiles but it fails to calibrate VIX smiles.

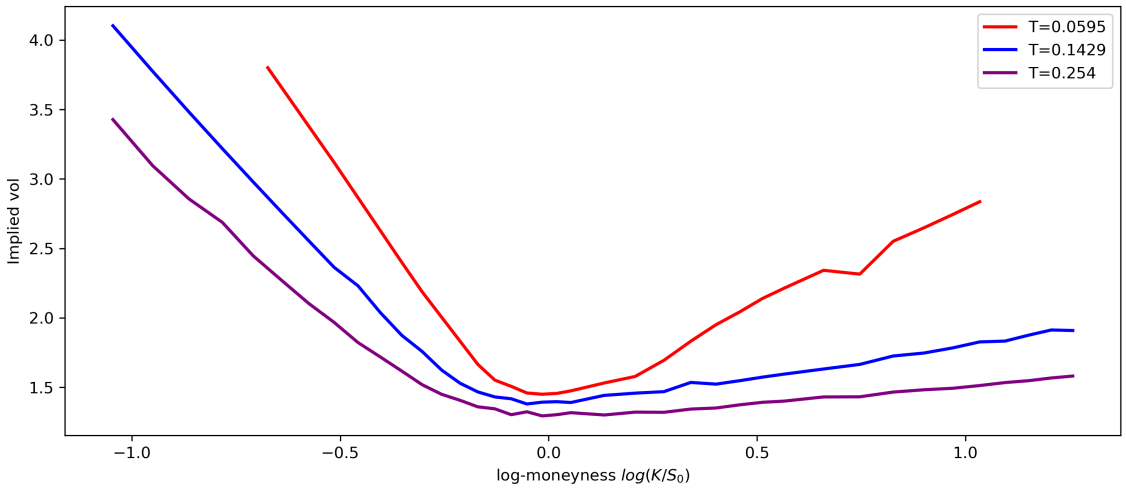

Figure 2.6: VIX volatility smiles as of July 14 2020, from Yahoo Finance website. T is time to expiry in years. The IV from the Yahoo finance dataset is actually the mean between the bid and ask implied volatilities.

2.2 The Generalized Rough Heston Model

Following the observations made in the first chapter, we consider the rough version of the well known Heston model. Our main goal is to implement an efficient pricing methodology that enables us to perform calibration over market data. Note that Monte-Carlo methods conduct to very long simulations due to the non-Markovian nature of the fractional Brownian motion.

The pricing method used within this model, relies on the simulation of the characteristic function expression of the log-price which is now the solution of a fractional Ricatti equation where a fractional derivative appears instead of a classical one within the Heston model.

Once values of the characteristic function over an equidistant partition are obtained, we apply the Lewis' approach that is based on the inverse Fourier transform to get the price of European Call options.

2.2.1 Specifications of the generalized rough Heston model

Although the Heston model reproduces several important stylised facts of low frequency price data, namely leverage effect, time-varying volatility and fat tails, and generates reasonable shapes and dynamics for the implied volatility surface, the first chapter of this paper suggests that the spot log-volatility process behaves like a fractional Brownian motion.

To introduce the rough Heston model, first recall the Mandelbrot-van Ness representation of a fractional Browian motion

$$W_t^H = \frac{1}{\Gamma(H+1/2)} \int_{-\infty}^{0} \left((t-s)^{H-1/2} - (-s)^{H-1/2} \right) dW_s + \frac{1}{\Gamma(H+1/2)} \int_0^t (t-s)^{H-1/2} dW_s, \tag{2.2.1}$$

where Γ denotes the Gamma function. Note that the kernel $(t-s)^{H-1/2}$ has an important impact on the rough dynamics of the fractional Brownian motion for $H < 1/2$. So in order to maintain a rough behaviour of the volatility in the Heston model, we introduce the kernel $(t-s)^{\alpha-1}$ in a Heston-like stochastic volatility process, with $\alpha = H + 1/2$. This yields to consider the rough generalization of the Heston model, called the rough Heston model which was first introduced by El Euch and Rosenbaum in [14] and [15].

This model satisfies the following dynamics for $(S_t)_{t\geq 0}$, the underlying price process

$$dS_t = S_t \sqrt{v_t} dW_t, \tag{2.2.2}$$

where W is a Brownian motion and v is the instantaneous variance.

Moreover, the instantaneous variance process $(v_t)_{t\geq 0}$ is defined as follows

$$v_t = v_0 + \int_0^t (t-s)^{\alpha-1} \frac{\lambda}{\Gamma(\alpha)} \left(\theta_0(s) - v_s \right) ds + \int_0^t (t-s)^{\alpha-1} \frac{\lambda\nu}{\Gamma(\alpha)} \sqrt{v_s} dB_s, \tag{2.2.3}$$

with $\langle W, B \rangle_t = \rho dt$. Hence ρ is the correlation between spot prices and volatility moves, so $\rho \in [-1, 1]$. ν is the volatility of volatility, so it is positive as well as λ. The mean reversion level parameter $\theta_0(.)$ is allowed to be an $\mathcal{F}_t$-measurable function which makes the model time consistent as explained in [16]. For the rest of the study, we consider θ_0 to be constant over the time for the sake of simplicity.

Furthermore, one can note that for such values of α, the rough Heston model is not Markovian and the variance process is no longer a semi-martingale. Finally it is straightforward to check that equation (2.2.3) leads to the classical Heston model with time-dependent mean reversion level when H tends to $1/2$.

The expression of the characteristic function of $X_t := log(S_t/S_0)$ within the generalized rough Heston model, which is the main result of [14, Section 4.2, Theorem 4.1], is as follows

$$\mathbb{E}\left[e^{iaX_t}\right] = exp\left\{ \int_0^t h(a, t-s) \left(\lambda\theta + \frac{V_0 s^{-\alpha}}{\Gamma(1-\alpha)} \right) ds \right\}. \tag{2.2.4}$$

Using a changement of variable of the form $u := t - s$ in the second term gives

$$\mathbb{E}\left[e^{iaX_t}\right] = exp\left\{\theta\lambda I^1 h(a,t) + V_0 I^{1-\alpha} h(a,t)\right\}, \tag{2.2.5}$$

where h is the unique continuous solution of the fractional Riccati equation

$$D^\alpha h(a,t) := F(a, h(a,t)) \quad \text{and} \quad I^{1-\alpha} h(a,0) = 0, \tag{2.2.6}$$

and

$$F(a,x) := -\frac{1}{2}(a^2 + ia) + \lambda(ia\rho\nu - 1)x + \frac{(\lambda\nu)^2}{2}x^2, \tag{2.2.7}$$

with D^α and $I^{1-\alpha}$ the fractional derivative and integral operators defined by

$$I^r f(t) := \frac{1}{\Gamma(r)}\int_0^t (t-s)^{r-1} f(s)ds \quad \text{and} \quad D^r f(t) := \frac{1}{\Gamma(1-r)}\frac{d}{dt}\int_0^t (t-s)^{-r} f(s)ds. \tag{2.2.8}$$

The main inconvenient is that such fractional Riccati equation does not have any explicit solution. However, it can be solved numerically.
But, why is the characteristic function of the log-price so important ? The knowledge of the characteristic function of such stochastic process allows us to determine Call prices by using Fourier inversion methods.

2.2.2 Numerical Scheme

One can demonstrate that the Riccati differential equation (2.2.6) can be transformed into the non-linear Volterra integral equation given by

$$h(a,t) = \frac{1}{\Gamma(\alpha)}\int_0^t (t-s)^{\alpha-1} F(a, h(a,s))ds. \tag{2.2.9}$$

To perform simulation we follow the numerical scheme explained in [17, Section 2] which describes the Adams-Bashforth method. For the sake of clarity, we note $g(a,t) = F\left(a, h(a,t)\right)$. Given the time interval $[0,T]$ and an equidistant partition $0 = t_0 \leq t_1 < ... < t_n = T$ with time increment Δ, we approximate $h(a, t_{k+1})$ by

$$h(a, t_{k+1}) \approx \frac{1}{\Gamma(\alpha)}\int_0^{t_{k+1}} (t_{k+1} - s)\hat{g}(a,s)ds, \tag{2.2.10}$$

and

$$\hat{g}(a,t) = \frac{t_{j+1} - t}{t_{j+1} - t_j}\hat{g}(a, t_j) + \frac{t - t_j}{t_{j+1} - t_j}\hat{g}(a, t_{j+1}), \quad t \in [t_j, t_{j+1}) \quad \text{with} \quad 0 \leq j \leq k. \tag{2.2.11}$$

One can see that the latter equation is only a trapezoidal discretization of the fractional integral. This gives the following scheme

$$\hat{h}(a, t_{k+1}) = \sum_{0 \leq j \leq k} a_{j,k+1} F\left(a, \hat{h}(a, t_j)\right) + a_{k+1,k+1} F\left(a, \hat{h}(a, t_{k+1}\right), \tag{2.2.12}$$

with

$$a_{0,k+1} := \frac{\Delta^\alpha}{\Gamma(\alpha+2)}\left(k^{\alpha+1} - (k-\alpha)(k+1)^\alpha\right), \tag{2.2.13}$$

$$a_{j,k+1} := \frac{\Delta^\alpha}{\Gamma(\alpha+2)}\left((k-j+2)^{\alpha+1} + (k-j)^{\alpha+1} - 2(k-j+1)^{\alpha+1}\right), \quad 1 \leq j \leq k, \tag{2.2.14}$$

$$a_{k+1,k+1} := \frac{\Delta^\alpha}{\Gamma(\alpha+2)}. \tag{2.2.15}$$

Note that $\hat{h}(a, t_{k+1})$ is present on both sides of the equation (2.2.12), making that scheme implicit. Hence, a preliminary estimation of $\hat{h}(a, t_{k+1})$ through Riemann sum is required in the righ-hand

side in order to determine a better approximation so that we can then use. It is denoted by $\hat{h}^P(a, t_{k+1})$ and defined as follows

$$\hat{h}^P(a, t_{k+1}) = \frac{1}{\Gamma(\alpha)} \int_0^t (t-s)^{\alpha-1} \tilde{g}(a, s) ds, \quad \text{with} \quad \tilde{g}(a, t) = \hat{g}(a, t_j), \text{ for } t \in [t_j, t_{j+1}), 0 \leq j \leq k, \tag{2.2.16}$$

Therefore, we approach the integral in (2.2.16) by the product rectangle rule. So we have:

$$\hat{h}^P(a, t_{k+1}) = \sum_{0 \leq j \leq k} b_{j,k+1} F\left(a, \hat{h}(a, t_j)\right), \tag{2.2.17}$$

and

$$b_{j,k+1} := \frac{\Delta^\alpha}{\Gamma(\alpha+1)} \left((k-j+1)^\alpha - (k-j)^\alpha\right), \quad 0 \leq j \leq k. \tag{2.2.18}$$

Finally, the explicit numerical scheme is

$$\hat{h}(a, t_{k+1}) = \sum_{0 \leq j \leq k} a_{j,k+1} F\left(a, \hat{h}(a, t_j)\right) + a_{k+1,k+1} F\left(a, \hat{h}^P(a, t_{k+1})\right), \quad \hat{h}(a, 0) = 0. \tag{2.2.19}$$

Convergence reasons are provided by Li and Tao in [18, Section 3.2, Theorem 3.4]. Moreover, we have the following properties

$$\max_{t_j \in [0,t]} |\hat{h}(a, t_j) - h(a, t_j)| = o(\Delta), \tag{2.2.20}$$

$$\max_{t_j \in [\epsilon,t]} |\hat{h}(a, t_j) - h(a, t_j)| = o(\Delta^{2-\alpha}), \quad \forall \epsilon > 0. \tag{2.2.21}$$

Then, the Lewis' method, based on the inverse Fourier transform and explained in Appendix (F.1), is applied to get the price of a European Call option given by

$$C(S_0, T, K) := \mathbb{E}^{\mathbb{P}}\left[(S_T - K)^+ | \mathcal{F}_0\right],$$

where K and T are respectively the strike price and the maturity date.

2.2.3 Fits to one trading day

In this section, we present the fits obtained with the generalized rough Heston model on both SPX and VIX implied volatility smiles.

Fits to the SPX implied volatility surface

In order to calibrate the parameter (H, ν, ρ), we consider the objective function given by

$$\sum_k \left(\sigma_k^{Hest}(H, \nu, \rho) - \sigma_k^{Yahoo}\right)^2, \tag{2.2.22}$$

subject to the following constraints

$$\begin{cases} H \in (0, 1/2], \\ \nu \geq 0, \\ \rho \in [-1, 1], \end{cases}$$

where $\sigma_k^{Hest}(H, \nu, \rho)$ and σ_k^{Yahoo} are respectively the implied volatilities from the rough Heston model and the Yahoo Finance dataset. Our aim is to minimize (2.2.22) which corresponds to the distance between the targeted implied volatilities and the ones from the generalized rough Heston model.

Figure (2.7) displays calibration results on the S&P implied volatility surface as of July 10, 2020. The following calibrated parameters are obtained

$$H = 0.012, \quad \lambda = 0.88, \quad \rho = -0.7, \quad V_0 = 0.148, \quad \nu = 0.96, \quad \theta = 0.016. \tag{2.2.23}$$

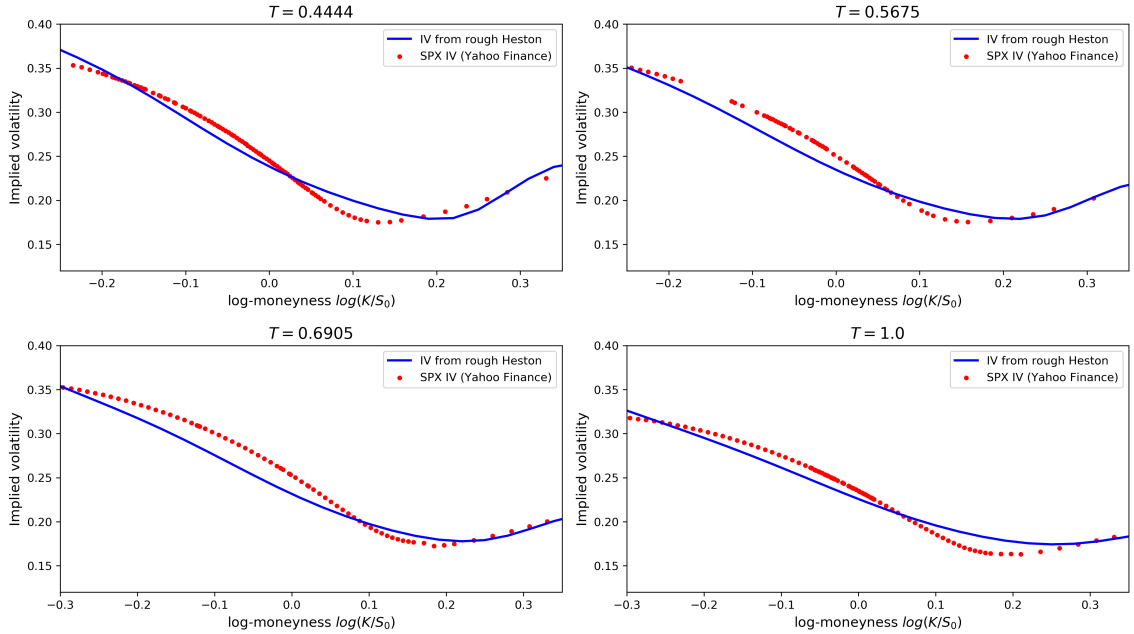

Figure 2.7: Volatility smiles as of July 10, 2020: red dots represent SPX implied volatilities and all the blue lines, coming from the same parameters, are from the rough Heston model. T is time to expiry in years. The IV from the Yahoo finance dataset is actually the mean between the bid and ask implied volatilities. $H = 0.012$.

However, note that it is very unlikely that the objective function admits a unique global minimum and may have several global minimums. Thus, this set of parameters could not be unique.

One can see that the generalized rough Heston model provides a good fit to the implied volatility surface. However, this fit is not as good as the one derived within the rough Bergomi model. Moreover, on this chosen day, H is close to zero, meaning that the volatility is particularly rough. But is it consistent with the value of H we observed when we studied stylized facts of the realized variance time series ? Recall that we shew that the behavior of historical log-volatility of the SPX index is similar to a fractional Brownian motion with small Hurst parameter of order 0.1. On both studies, we retrieve that the calibrated values of H are small.

Figure (2.8) presents curves coming from the rough Heston model as well, but the calibration was this time performed with the value of H equals to the SPX Hurst index derived when we studied stylized facts of the realized variance time series.

Regarding the at-the-money volatility skew, recall that it is defined to be the first derivative of the implied volatility with respect to the strike price K. Moreover, throughout the study, we estimated it by using the finite difference method, see equation (2.2.24).

$$\psi(\tau) := \left.\frac{\partial \sigma_{iv}(K,\tau)}{\partial K}\right|_{K=S_t} \approx \frac{\sigma_{iv}(S_t+\epsilon,\tau) - \sigma_{iv}(S_t-\epsilon,\tau)}{2\epsilon}. \tag{2.2.24}$$

Based on the paper [19] by Fukasawa, Omar El Euch demonstrated in [15, Section 4, Theorem 3] that the asymptotic expansion of the ATM volatility skew is given by

$$\left.\frac{\partial \sigma_{iv}(K,\tau)}{\partial K}\right|_{K=S_t} = g(\theta)\theta^{H-1/2} + o\left(\theta^{2H-1/2}\right) \tag{2.2.25}$$

where g is a bounded function. Such asymptotic expansion allows us to compare the term structure of the ATM volatility skew to empirical ATM volatility of the SPX, see Figure (2.9).

Finally, Figure (2.7) and Figure (2.9) display that the generalized rough Heston model, developed in [15], is consistent with historical implied volatility data. However, one main concern remains: Does the generalized rough Heston model allow us to calibrate jointly SPX and VIX smiles ?

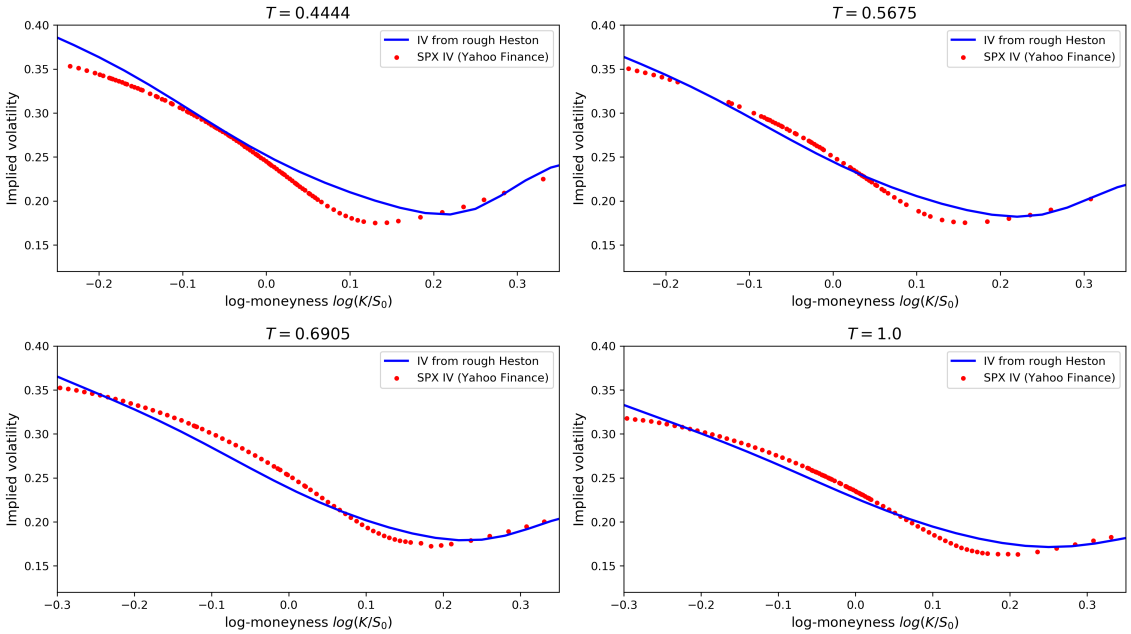

Figure 2.8: Volatility smiles as of July 10, 2020: red dots represent SPX implied volatilities and all the blue lines, coming from the same parameters, are from the rough Heston model. T is time to expiry in years. The IV from the Yahoo finance dataset is actually the mean between the bid and ask implied volatilities. $H = 0.11$.

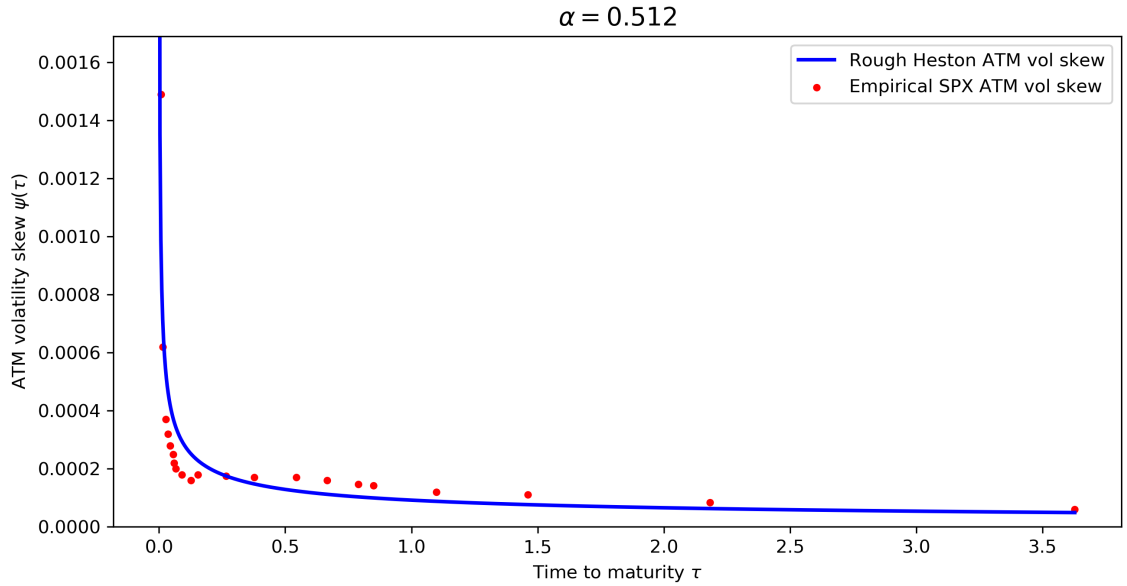

Figure 2.9: ATM Volatility skews as of June 15, 2020: red dots represent empirical SPX ATM volatility skew and the blue line is from the rough Heston model. τ is time to expiry in years.

Fits to the VIX implied volatility surface

Following the fits obtained previously to the SPX smiles, we now check whether or not it is possible to jointly calibrate SPX and VIX smiles. To do so, we first calibrate the rough Heston model to VIX implied volatility surface. We got the following parameters

$$H = 0.04, \quad \lambda = 0.96, \quad \rho = -0.6, \quad V_0 = 2.2, \quad \nu = 0.96, \quad \theta = 3.0. \tag{2.2.26}$$

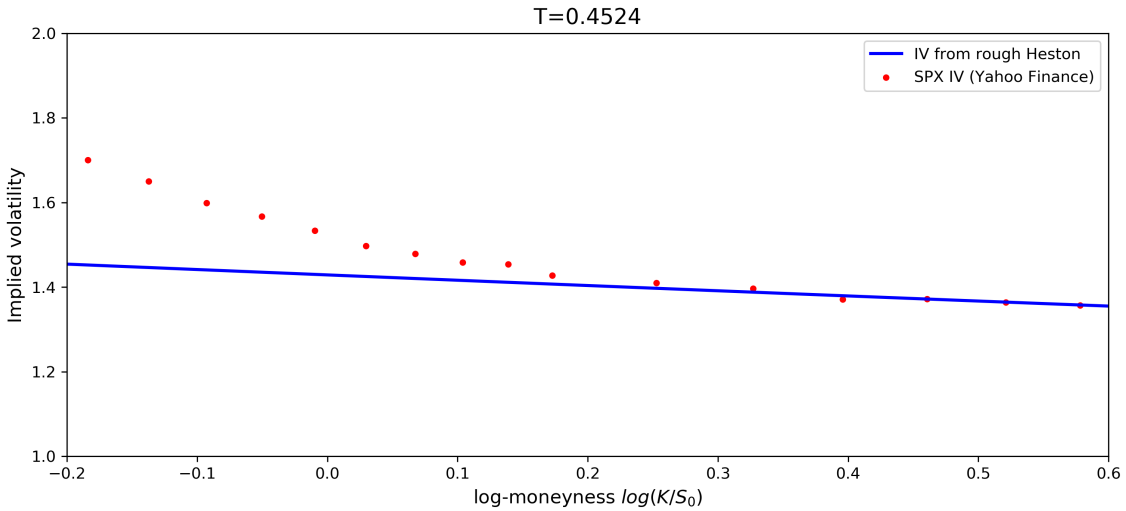

Figure 2.10: Volatility smiles as of July 10, 2020: red dots represent VIX implied volatilities and the blue line, coming from the same parameters, are from the rough Heston model. T is time to expiry in years. The IV from the Yahoo finance dataset is actually the mean betweenthe bid and ask implied volatilities.

Finally, Figure (2.10) shows that the rough Heston model does not reproduce extreme left tails. Furthermore, one can note that the parameters obtained for this plot are very different from the ones used to fit the model to the SPX smiles. Nevertheless, this set of parameters in (2.2.26) can somehow be close to a global minimum of the objective function applied to SPX historical data. Therefore, those parameters from (2.2.26) were used to fit SPX smiles, but the result is far from being acceptable. The parameters obtained from the SPX calibration do not provide a good fit to the VIX smiles either. Hence, the rough Heston model fails to calibrate jointly the two implied volatility surfaces.

2.3 The Quadratic Rough Heston Model

Although the rough volatility models tested so far fit the volatility surface remarkably well with very few parameters, they fail to fit jointly SPX and VIX implied volatility surfaces. Actually, designing a model that simultaneously calibrates SPX and VIX options prices is known to be extremely challenging and complex. However, Jim Gatheral et al. in [8, Section 3] introduced a model with continuous SPX and VIX paths that enables us to fit SPX and VIX options smiles simultaneously.

2.3.1 Specification of the Quadratic Rough Heston model

Julien Guyon, an active researcher in rough volatility modeling, stated that calibrating jointly SPX and VIX with a continuous sample-paths model may not be possible. However, in March 2019, he introduced a necessary condition for a continuous model to fit simultaneously SPX and VIX smiles: The inversion of convex ordering between volatility and the local volatility implied by option prices, see [20] and [21].

This led Jim Gatheral and his coauthors in [8] to consider super-Heston rough volatility models, developed in [22], that present the particular feature of being consistent with the strong Zumbach effect. It characterizes models where the conditional dynamics of volatility with respect to the past depend not only on the past volatility trajectory but also on the historical price path. Therefore, such effect could be seen as the required condition formulated by Julien Guyon to fit simultaneously SPX and VIX smiles.

That's why the quadratic rough Heston model that we consider from now, is a special case of the super-Heston rough models of [22].

The dynamics of the underlying price process $(S_t)_{t\geq 0}$ and its instantaneous variance $(v_t)_{t\geq 0}$ are defined as follows

$$dS_t = S_t\sqrt{v_t}dW_t, \tag{2.3.1}$$
$$v_t = a(Z_t - b)^2 + c, \tag{2.3.2}$$

with W a standard Brownian motion and a, b, c three positive constants which can be interpreted the following way:

- a represents the sensitivity of the volatility to the feedback of price returns. Therefore, the greater a is, the higher is the volatility of volatility.
- b is related to the asymmetry of the feedback effect. Note that the same absolute value of Z, volatility is higher when Z is negative. Such asymmetry enables us to better estimate the empirical behavior of the VIX.
- c is the minimal instantaneous variance used to shift upward or downward simulated volatility smiles.

Finally, the process $(Z_t)_{t\geq 0}$ follows a rough Heston model

$$Z_t = \int_0^t (t-s)^{\alpha-1}\frac{\lambda}{\Gamma(\alpha)}(\theta_0(s) - Z_s)ds + \int_0^t (t-s)^{\alpha-1}\frac{\lambda}{\Gamma(\alpha)}\eta\sqrt{v_s}dW_s, \tag{2.3.3}$$

with $\alpha \in (1/2, 1)$, $\lambda > 0$, $\eta > 0$ (which is the volatility of volatility) and θ_0 a deterministic function. Note that the only source of randomness comes from W. Thus the volatility is driven only by the price dynamics, making that model a pure-feedback model.

The paper [8] presents additional interesting features of this model. Indeed, it highlights the path-dependent trait of the process Z, which suggests that the volatility depends on recent price changes. Furthermore, it is also shown that Z is highly sensitive to recent returns meaning that long periods of trends or sudden upwards or downwards moves of the price generate large values for $|Z|$ and so high volatility, above all when Z is negative.

2.3.2 Numerical Scheme

Monte-Carlo Scheme

In order to perform simulation, we first consider θ_0 equals to the following function

$$\theta_0(s) = \frac{Z_0}{\lambda\Gamma(1-\alpha)} s^{-\alpha}. \tag{2.3.4}$$

Although this restriction reduces the complexity of the simulation, it also prevents us from reaching better fits.

Inserting this expression of θ_0 into (2.3.3) simplifies the definition of the process Z. The latter becomes

$$Z_t = Z_0 - \int_0^t (t-s)^{\alpha-1} \frac{\lambda}{\Gamma(\alpha)} Z_s ds + \int_0^t (t-s)^{\alpha-1} \frac{\lambda}{\Gamma(\alpha)} \eta \sqrt{v_s} dW_s, \quad t \geq 0. \tag{2.3.5}$$

Furthermore, by applying Ito's formula to the process S, we have

$$S_t = S_0 exp\left\{ \int_0^t \sqrt{v_s} dW_s - \frac{1}{2} \int_0^t v_s ds \right\}, \quad t \geq 0. \tag{2.3.6}$$

Before introducing the numerical scheme, we first need to consider the following equidistant partition $0 = t_0 < t_1 < ... < t_n = T$ with Δ the time increment. The integer M denotes the number of paths generated. Finally our simulation procedure is as follows:

1. We first generate the covariance matrix of the Brownian motion W over the partition $t_0 < t_1 < ... < t_n$.

2. We then use the Cholesky decomposition of this covariance matrix to get the matrix $(W_{t_i,m})_{0 \leq i \leq n, 1 \leq m \leq M}$ of the realisations of W. Thus, one column of this matrix corresponds to one path of the Brownian motion.

3. Given the latter matrix, we can then construct the matrix of the processes Z and v by using Riemann sums to estimate the integrals. So we have:

$$Z_{t_i,m} = Z_0 - \frac{\lambda\Delta}{\Gamma(\alpha)} \sum_{j=0}^{i-1} (t_i - t_j)^{\alpha-1} Z_{t_j,m} + \frac{\lambda\eta}{\Gamma(\alpha)} \sum_{j=0}^{i-1} (t_i - t_j)^{\alpha-1} \sqrt{v_{t_j,m}} \left(W_{t_{j+1},m} - W_{t_j,m} \right), \tag{2.3.7}$$

   with

$$v_{t_j,m} = a(Z_{t_j,m} - b)^2 + c, \quad 1 \leq m \leq M, \tag{2.3.8}$$

   and Δ the time increment.

4. Given the matrix of the volatility process, we can compute the stock prices $(S_{T,m})_{1 \leq m \leq M}$ by using

$$S_{T,m} = S_0 exp\left\{ \sum_{i=0}^{n-1} \sqrt{v_{t_i,m}} \left(W_{t_{i+1},m} - W_{t_i,m} \right) - \frac{\Delta}{2} \sum_{i=0}^{n-1} v_{t_i,m} \right\}. \tag{2.3.9}$$

Once the latter step is implemented, then we are now able to derive the Call price $C(S(0), t, K) := \mathbb{E}\left[(S_t - K)^+\right]$

Hybrid Scheme

Otherwise, the Riemann sum approach does not take into account the explosion near zero of the kernel function in the following stochastic Volterra process (introduced in 2.3.5):

$$V_t^\alpha := \int_0^t (t-s)^{\alpha-1} \frac{\lambda}{\Gamma(\alpha)} \eta \sqrt{v_s} dW_s. \tag{2.3.10}$$

Hence, we recommend to use the hybrid scheme introduce in [4, Section 2.3], and already used in the implementation of the rough Bergomi model.

So as to simulate the process $(V_t^\alpha)_{t\geq 0}$ efficiently and accurately, we consider the first-order variant ($\kappa = 1$) of the hybrid scheme which is based on the approximation

$$\tilde{V}_{t_i}^\alpha := \int_{(i-1)\Delta}^{i\Delta} (i\Delta - s)^{\alpha-1} \frac{\lambda}{\Gamma(\alpha)} \eta \sqrt{v_s} dW_s + \sum_{k=2}^{i} (\Delta b_k)^{\alpha-1} \frac{\lambda}{\Gamma(\alpha)} \eta \sqrt{V_{(i-k)\Delta}} \left(W_{(i-k+1)\Delta} - W_{(i-k)\Delta} \right), \tag{2.3.11}$$

with

$$b_k := \left(\frac{k^\alpha - (k-1)^\alpha}{\alpha} \right)^{\frac{1}{\alpha-1}}. \tag{2.3.12}$$

2.3.3 Fits to one trading day

Fits to the SPX volatility smiles

We first calibrate our model with the SPX implied volatility surface of the 20^{th} July 2020 and of the 10^{th} August 2020 by using respectively Riemann sum approach and the hybrid scheme approximation, see Figures (2.11) and (2.12). We considered the same objective function used to calibrate the generalized rough Heston model.

Considering the Riemann scheme approximation, we obtain the following parameters

$$H = 0.04, \quad \lambda = 1.1, \quad \eta = 1.1, \quad Z_0 = 0.05, \quad a = 0.384, \quad b = 0.095, \quad c = 0.020. \tag{2.3.13}$$

Recall that it is very unlikely that the objective function admits a unique global minimum and may have several global minimums. Thus, this set of parameters could not be unique.

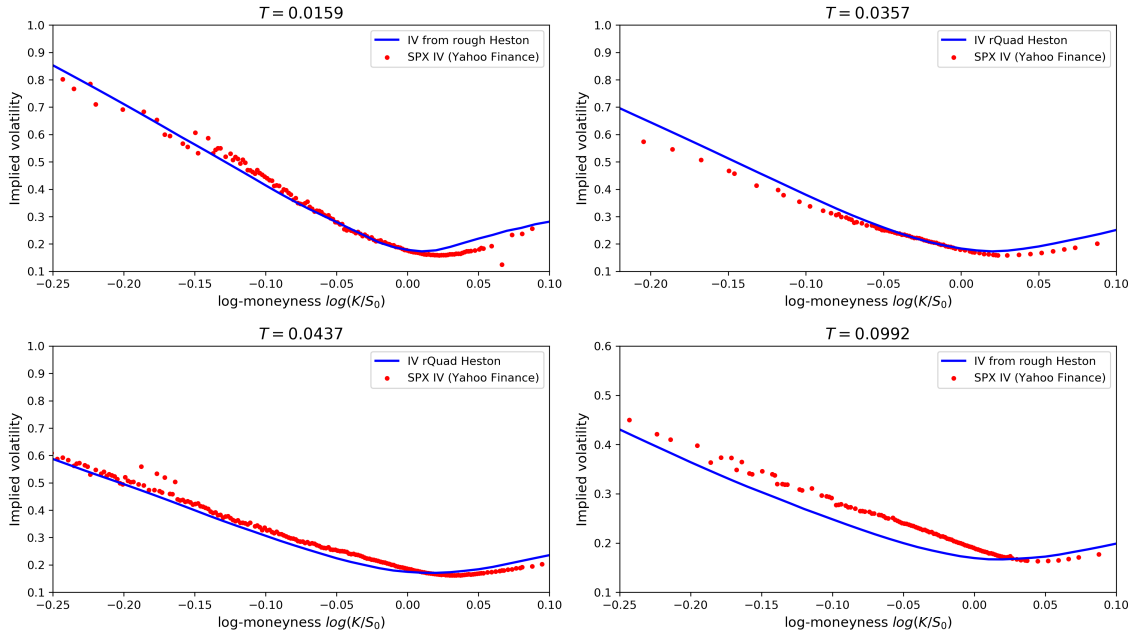

Figure 2.11: Volatility smiles as of July 20, 2020: red dots represent SPX implied volatilities and all the blue lines, coming from the same parameters, are from the quadratic rough Heston model (with Riemann sum). T is time to expiry in years. The IV from the Yahoo finance dataset is actually the mean between the bid and ask implied volatilities.

Regarding the implementation of the quadratic rough Heston model with the hybrid scheme, the parameters are as follows

$$H = 0.04, \quad \lambda = 1.1, \quad \eta = 1.1, \quad Z_0 = 0.05, \quad a = 0.384, \quad b = 0.095, \quad c = 0.013. \tag{2.3.14}$$

Note that only the parameter c has changed over the two plots.

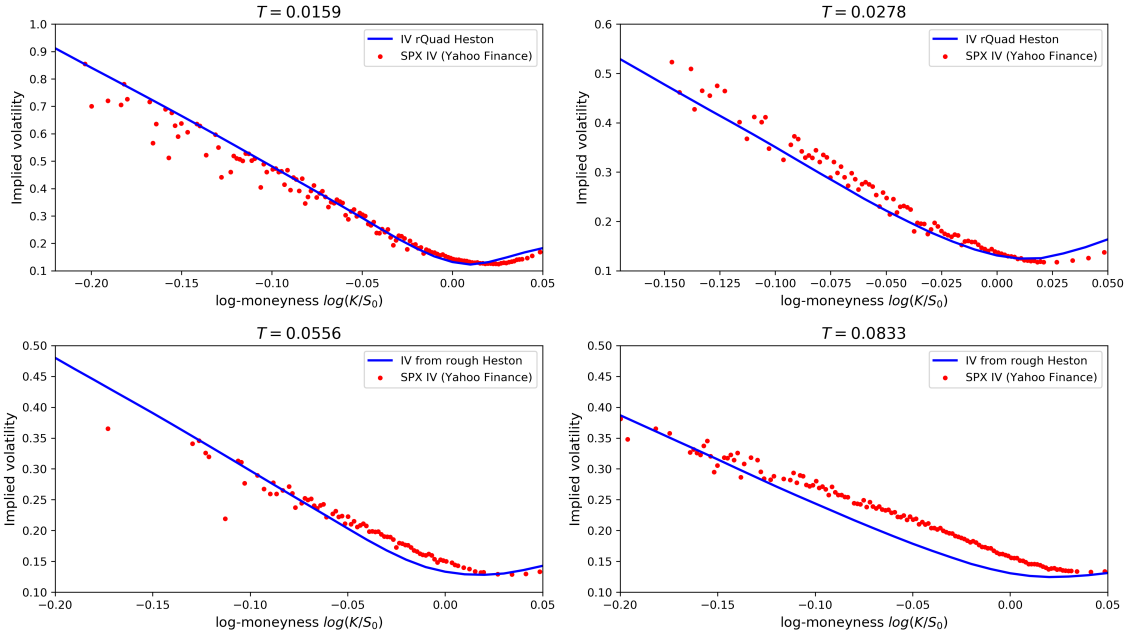

Figure 2.12: Volatility smiles as of August 10, 2020: red dots represent SPX implied volatilities and all the blue lines, coming from the same parameters, are from the quadratic rough Heston model (with Hybrid scheme). T is time to expiry in years. The IV from the Yahoo finance dataset is actually the mean between the bid and ask implied volatilities.

Figures (2.11) and (2.12) highlight that the calibrated model reproduces very well the overall shape of the SPX implied volatility surface even though we restricted the expression of θ_0 for the sake of simplicity.

In order to make the calibration algorithm faster, note that we can always consider $\eta = 1$ up to a rescaling of the other parameters.

Fits to the VIX volatility smiles

To fit the VIX implied volatility smiles, all the parameters stay unchanged, except c. Recall that c is only the minimal instantaneous variance used to shift upward or downward simulated volatility smiles. We illustrate the performances of the model by considering the two dates mentioned in the previous section and the two methods, Riemann sum and hybrid scheme, to simulate the Volterra process.

Figure (2.13), with $c = 1.8$, shows that the fits are quite impressive apart from the plot with the lowest expiration time T. Regarding Figure (2.14), with $c = 2.3$, the fits are good as well. Note that we did not plot fits for $T > 0.0635$ because the dataset from Yahoo finance did not provide acceptable curves.

One can observe on (2.13) and (2.14) that the model still struggles to fit extreme left tails.

Given that the same parameters (except c) are used to plot VIX and SPX smiles from the quadratic rough Heston model, one could suggest that the quadratic rough Heston model is **almost** able to calibrate jointly the SPX and VIX implied volatility surfaces.
However Jim Gatheral et al. shew that the quadratic rough Heston model can fit jointly both volatility surfaces with the same set of parameters $(H, \lambda, Z_0, a, b, c)$. Hence, one question remains, to what extent is a model said to be able to fit jointly SPX and VIX implied volatility smiles ? Should every parameter stay unchanged across the underlyings although the smiles are very different ?

In our situation, with the datasets used above to perform calibrations, the VIX and SPX smiles are clearly different in terms of y-axis range, hence shifting upward or downward the smiles, then changing c is **necessary** to fit both implied volatility surfaces.

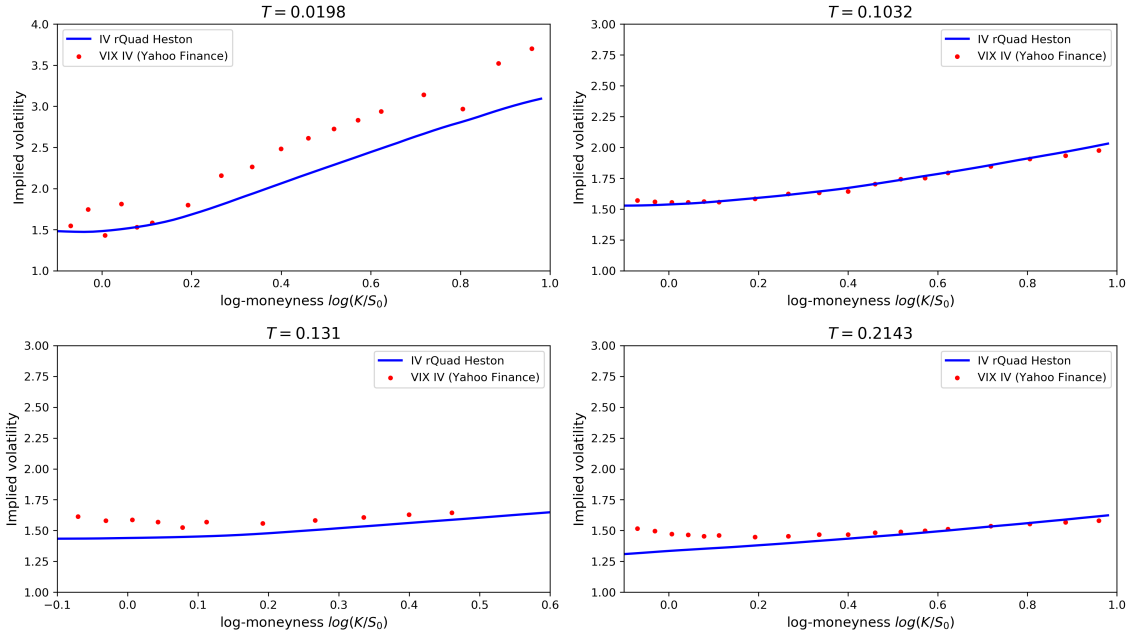

Figure 2.13: Volatility smiles as of July 20, 2020: red dots represent VIX implied volatilities and all the blue lines, coming from the same parameters, are from the quadratic rough Heston model (with Riemann sum). T is time to expiry in years. The IV from the Yahoo finance dataset is actually the mean between the bid and ask implied volatilities.

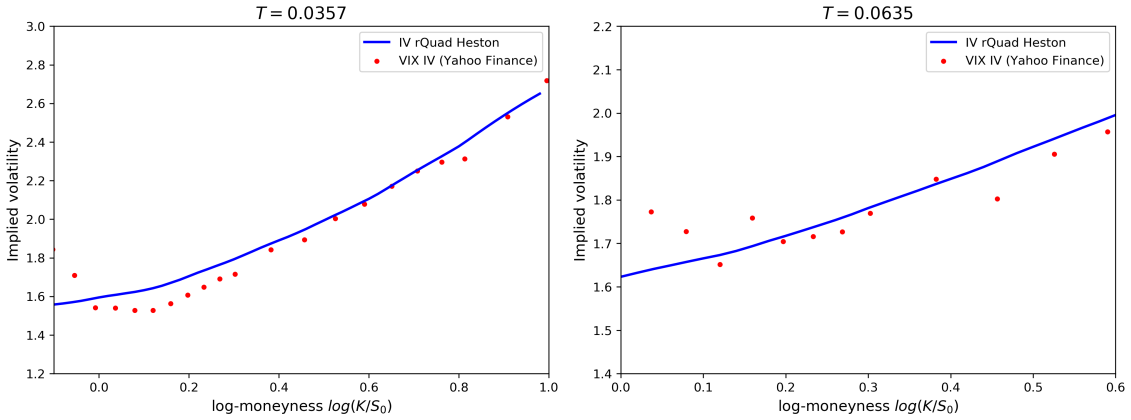

Figure 2.14: Volatility smiles as of August 10, 2020: red dots represent VIX implied volatilities and all the blue lines, coming from the same parameters, are from the quadratic rough Heston model (with Hybrid scheme). T is time to expiry in years. The IV from the Yahoo finance dataset is actually the mean between the bid and ask implied volatilities.

Conclusion

In this master thesis, we explored the rough nature of the spot log-volatility and the calibration of rough stochastic volatility pricing models using historical market data from Yahoo Finance.

By studying the sample moments of log-volatility increments, we shew that the spot log-volatility process behaves as a fractional Brownian motion with Hurst index $0 < H < 1/2$. Such dynamics of the log-volatility reproduces the properties of the historical time series of the volatility and provide a good fit to implied volatility surface for a wide range of different underlying assets as well.

The calibrations of rough stochastic volatility models show that such models outperform conventional Markovian model, even though they have very few parameters. Although the rough Bergomi model cannot fit VIX smiles, it provides impressive fits to SPX implied volatility surface by using the hybrid scheme method. Calibration plots from the rough Heston model obtained thanks to the Adams numerical scheme combined to the Lewis' approach are good as well, but this model does not allow us to simultaneously calibrate VIX/SPX smiles. Finally, unlike the two previous models, the quadratic rough Heston model enabled us to **almost** calibrate jointly both underlying assets. However, Jim Gatheral et al. in [8, Section 4] were able to calibrate jointly VIX and SPX smiles with the exact same set of parameters. Does this difference between our observations and the results from [8] come from the datasets used ? The VIX smiles from Yahoo Finance that we considered in this report are much higher than the ones used for calibrations in [8]. Hence, changing the parameter c in our case seems relevant and necessary to fit jointly both implied volatility surfaces. This issue raises the following questions: to what extent could we say that a model is able to calibrate jointly SPX and VIX smiles ? Could this property depend on the dataset considered ?

Continuous sample-paths models under rough volatility remain a major challenge in quantitative finance, and there is still a lot of room for exploration and improvements, especially in terms of fast and joint calibration approach.

Appendix A

Estimations of H

A.1 On different indices

Index	Estimates of H	Estimates of ν
SPX2.rk	0.117594	0.341476
FTSE2.rk	0.139819	0.266099
N2252.rk	0.095530	0.338894
GDAXI2.rk	0.137016	0.282929
RUT2.rk	nan	nan
AORD2.rk	0.079685	0.359848
DJI2.rk	0.114622	0.336430
IXIC2.rk	0.120033	0.299165
FCHI2.rk	0.124703	0.290940
HSI2.rk	0.099976	0.282359
KS11.rk	0.116545	0.283993
AEX.rk	0.131631	0.292246
SSMI.rk	0.154811	0.235868
IBEX2.rk	0.123253	0.285950
NSEI.rk	0.115257	0.315873
MXX.rk	0.092918	0.307996
BVSP.rk	0.099532	0.306327
GSPTSE.rk	nan	nan
STOXX50E.rk	0.118323	0.312451
FTSTI.rk	0.105314	0.230195
FTSEMIB.rk	0.122902	0.303811

Table A.1: Estimates of H and ν for all indices in the Oxford-Man Institute dataset.

A.2 On different time intervals

Index	H (first half)	H (second half)
SPX2.rk	0.091954	0.123571
FTSE2.rk	0.110710	0.164393
N2252.rk	0.099650	0.091936
GDAXI2.rk	0.121706	0.145583
RUT2.rk	0.079832	nan
AORD2.rk	0.056900	0.100327
DJI2.rk	0.100371	0.112462
IXIC2.rk	0.083168	0.132130
FCHI2.rk	0.109327	0.132300
HSI2.rk	0.100327	0.091861
KS11.rk	0.126736	0.095671
AEX.rk	0.111820	0.139942
SSMI.rk	0.137252	0.163870
IBEX2.rk	0.108333	0.131766
NSEI.rk	0.115666	0.115225
MXX.rk	0.075540	0.103705
BVSP.rk	0.075484	0.114195
GSPTSE.rk	nan	0.140437
STOXX50E.rk	0.102180	0.128748
FTSTI.rk	0.059519	0.136346
FTSEMIB.rk	0.102633	0.134533

Table A.2: Estimates of H over two different time intervals for all indices in the Oxford-Man Institute dataset.

Appendix B

Simulation of the Volterra process

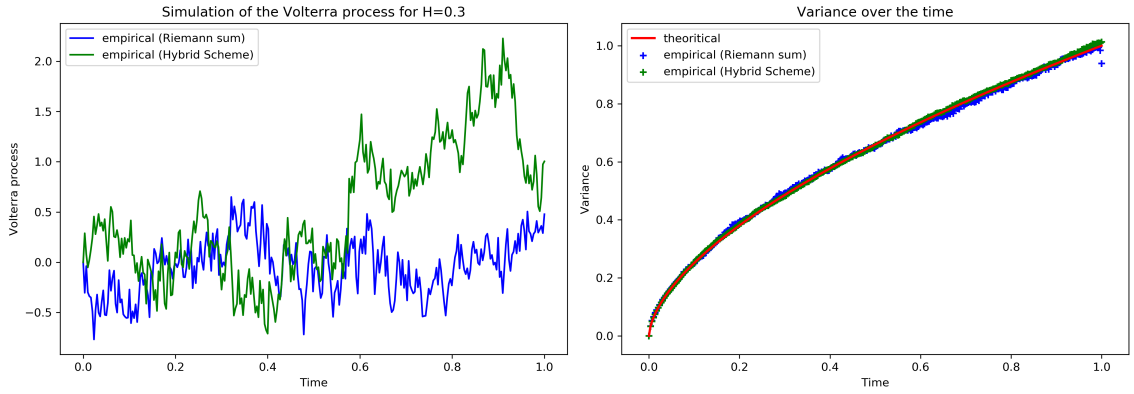

(a)

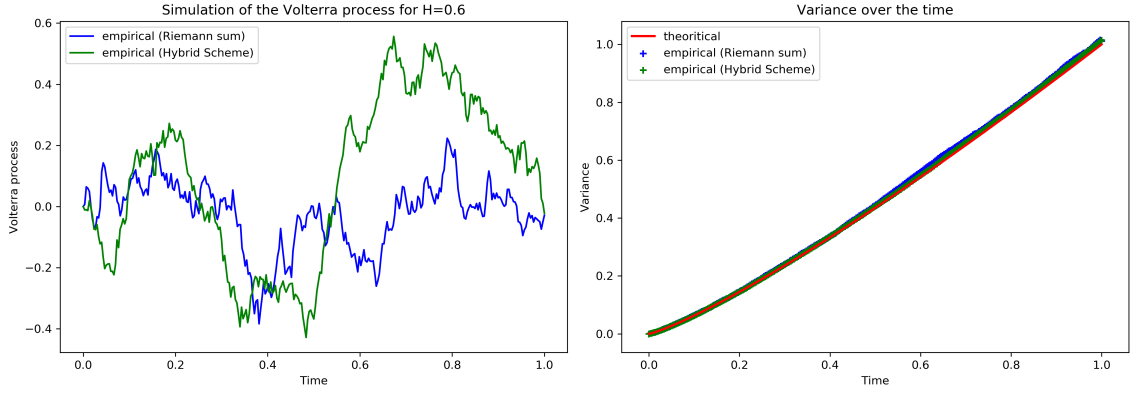

(b)

Figure B.1: (a) $H = 0.3$ (b) $H = 0.6$

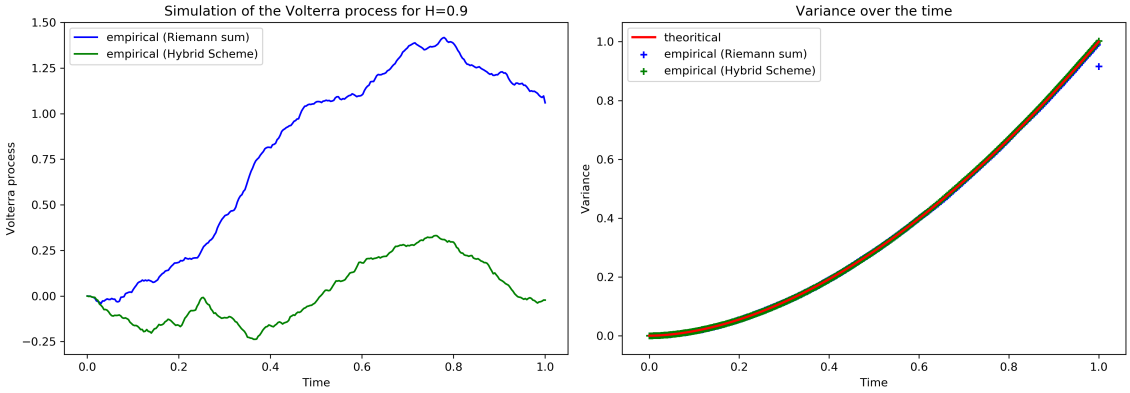

Figure B.2: $H = 0.9$

Appendix C

Underlying price process within the rough Bergomi model

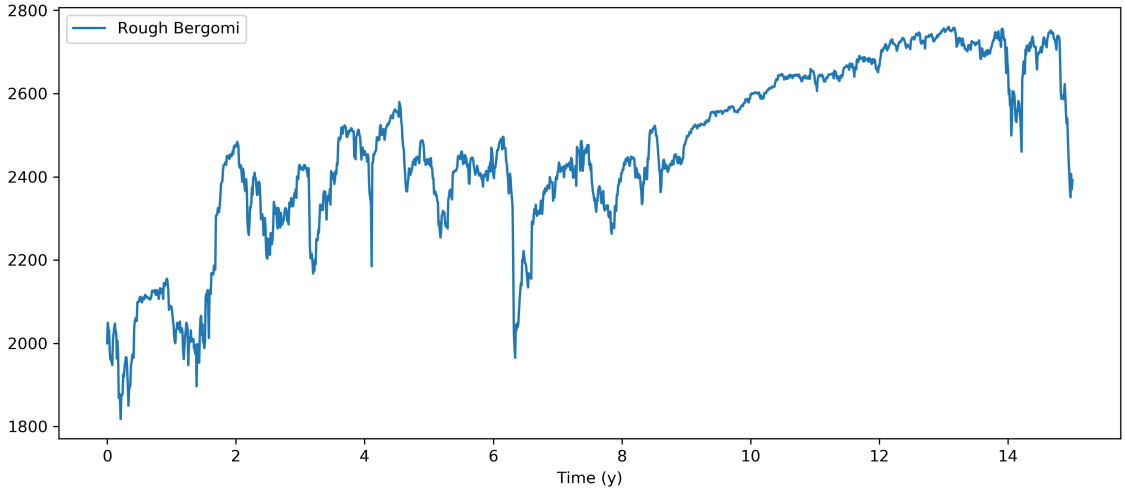

(a)

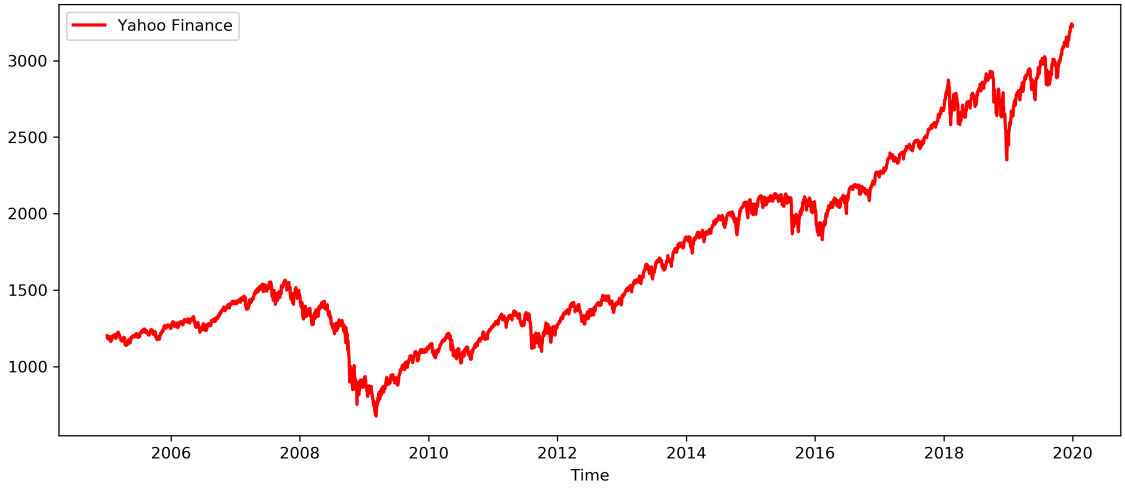

(b)

Figure C.1: (a) S&P 500 index from simulation of the rough Bergomi model (b) S&P 500 index from 1 January 2005 to 1 January 2020.

Appendix D

Spot volatility process within the rough Bergomi model

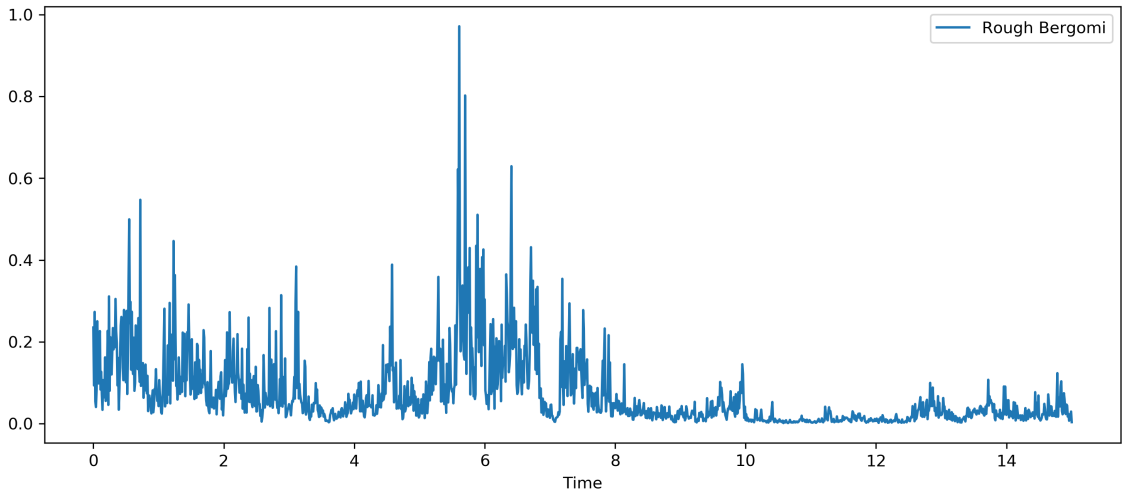

(a)

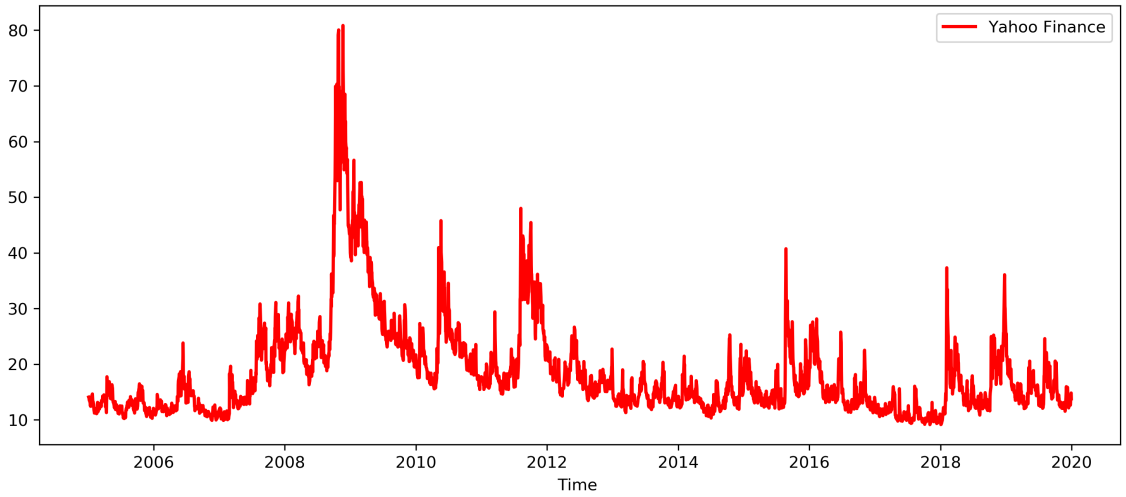

(b)

Figure D.1: (a) Spot volatility from simulation of the rough Bergomi model (b) Volatility index (VIX) from 1 January 2005 to 1 January 2020.

Appendix E

Fractional Brownian motion

E.1 Properties

Definition E.1.1 (Fractional Brownian Motion)**.** A fractional Brownian motion $\left\{W_t^H, t \geq 0\right\}$ is the generalisation of a Brownian motion. It is a continuous and centered Gaussian process with stationary increments, however, its increments are not independent, unlike the usual Brownian motion. Its covariance matrix is given by

$$\mathbb{E}\left[W_t^H W_s^H\right] = \frac{1}{2}\left(|t|^{2H} + |s|^{2H} - |t-s|^{2H}\right), \tag{E.1.1}$$

where $t \geq 0$, $s \geq 0$ and $0 < H < 1$ is the Hurst index.

Remark E.1.2. Note that the definition written above is enough to define the distribution of a Gaussian process since it is uniquely determined by its mean and covariance function.

Proposition E.1.1. *A fractional Brownian motion is said to be self-similar, i.e* $W_{aT}^H \overset{\mathcal{L}}{\approx} a^H W_T^H$ *for any positive constant* a*.*

Corollary E.1.3. *Given the definition of a FBM, one can see that:*

- *For* $H = 1/2$*:* $\mathbb{E}\left[W_t^{\frac{1}{2}} W_s^{\frac{1}{2}}\right] = t \wedge s$*, hence* $W^{\frac{1}{2}} = B$*, with* B *a Brownian motion.*
- *For* $H < 1/2$*: The increments are negatively correlated.*
- *For* $H > 1/2$*: The increments are positively correlated.*

Proposition E.1.2 (Mandelbrot-Van Ness representation)**.** *Let* $0 < H < 1/2$ *and* $\gamma = 1/2 - H$*. The Mandelbrot-Van Ness representation of fractional Brownian motion* $(W_t^H)_{t\in\mathbb{R}}$ *in terms of Wiener integrals is given by*

$$W_t^H = C_H \left\{\int_{-\infty}^{t} \frac{dW_s^{\mathbb{P}}}{(t-s)^{\gamma}} - \int_{-\infty}^{0} \frac{dW_s^{\mathbb{P}}}{(-s)^{\gamma}}\right\}, \tag{E.1.2}$$

For an in-depth introduction to fractional Brownian motions we refer the readers to [23].

E.2 Simulation of FBM

In order to simulate the values of a FBM $(W_t^H)_{t\geq 0}$ at the grid points $t_1 < ... < t_N$, the Cholesky decomposition is implemented.

1. We create the covariance matrix Σ following the equation (E.1.1).
2. Using the Cholesky decomposition, we got the lower triangular matrix L such that $\Sigma = LL^T$. Recall that this decomposition is possible if and only if Σ is positive definite.
3. Generate Z, a N-dimensional standard Gaussian vector.

4. Set $\hat{Z} = \Sigma Z$, where $\hat{Z}$ is a sample path of the FBM W^H.

Figure (E.1) clearly shows that the higher the Hurst parameter is, the smoother the curve will be.

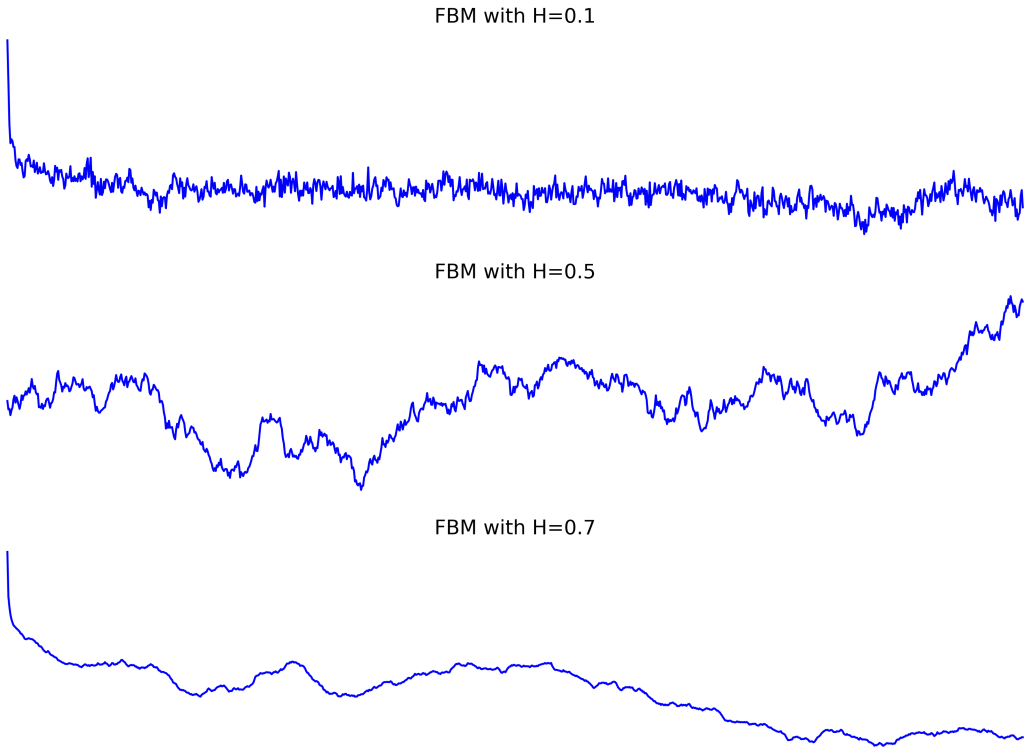

Figure E.1: Simulation of a fractional Brownian motion, using Cholesky decomposition.

Remark E.2.1. Although the Cholesky decomposition leads to an exact simulation, such method is expensive in terms of computation. It has a complexity of order $\mathcal{O}(N^3)$.

Appendix F

Pricing method

F.1 Lewis' approach

We present now a method based on the inverse Fourier transform applied on the characteristic function of the log-price process, explained in [24, Section 4.5] to derive Call prices in the specific case of the generalized rough Heston model. Let the function g be defined as follows:

$$g(x) = (x - e^k)^+ \quad \text{with} \quad x = log(S_t). \tag{F.1.1}$$

The Fourier transformation of g, denoted by $\mathcal{F}[g(x)]$, is given by

$$\mathcal{F}[g(x)] = \int_{-\infty}^{+\infty} e^{izx} g(x) dx =: \hat{g}(z). \tag{F.1.2}$$

However, since g is an unbounded function, the latter integral can not be finite. This issue can be bypassed by considering an exponential damping factor. Hence for some appropriate z_i we have $g(x)e^{-z_i x} = o\left(\frac{1}{x^2}\right)$. This justifies the existence of the Fourier transform along a line in the complex plane where the path of integration is parallel to the real axis. Some algebras give

$$\begin{aligned}
\hat{g}(z) &:= \int_{-\infty}^{+\infty} e^{izx} g(x) dx, \\
&= \int_{ln(K)}^{+\infty} e^{izx} (x - e^k) dx, \\
&= -\frac{K^{iz+1}}{z^2 - iz},
\end{aligned} \tag{F.1.3}$$

with z a complex.

The inverse Fourier transform allows us to recover the payoff function:

$$g(x) = \frac{1}{2\pi} \int_{iz_i - \infty}^{iz_i + \infty} e^{-izx} \hat{g}(z) dz. \tag{F.1.4}$$

Plugging (F.1.4) in the expression of the Call option yields

$$\begin{aligned}
C(S(0), T, K) &:= e^{-rT} \mathbb{E}^{\mathbb{Q}}[g(x)], \\
&= \frac{e^{-rT}}{2\pi} \mathbb{E}^{\mathbb{Q}} \left[\int_{iz_i - \infty}^{iz_i + \infty} e^{-izx} \hat{g}(z) dz \right], \\
&= \frac{e^{-rT}}{2\pi} \int_{iz_i - \infty}^{iz_i + \infty} \mathbb{E}^{\mathbb{Q}} \left[e^{-izx} \right] \hat{g}(z) dz, \\
&= \frac{e^{-rT}}{2\pi} \int_{iz_i - \infty}^{iz_i + \infty} \phi_T(-z) \hat{g}(z) dz.
\end{aligned} \tag{F.1.5}$$

Applying the payoff transform of a Call option in (F.1.5), we have

$$C(S(0), T, K) = -\frac{K e^{-rT}}{2\pi} \int_{iz_i - \infty}^{iz_i + \infty} \phi_T(-z) \frac{e^{izk}}{z^2 - iz} dz, \quad \text{with} \quad k = log\left(\frac{K}{S_0}\right). \tag{F.1.6}$$

By moving the integration contour to $z_i \in (0,1)$ and according to the Residue Theorem, the Call option value must equal the integral along $\Im(z) = z_i$ minus $2\pi i$ times the residue at $z = i$ which is S_0. This gives the following formula:

$$C\left(S(0), T, K\right) = S_0 - \frac{Ke^{-rT}}{2\pi} \int_{iz_i-\infty}^{iz_i+\infty} \phi_T(-z) \frac{e^{izk}}{z^2 - iz} dz. \tag{F.1.7}$$

A convenient choice is to shift the contour by $z_i = 1/2$, because then the path of integration is symmetrically located between the two poles. The change of variables $z = u + \frac{i}{2}$ and employing the symmetry property for real valued functions give

$$C\left(S(0), T, K\right) = S_0 - \frac{\sqrt{KS_0}e^{-rT/2}}{\pi} \int_0^{+\infty} \Re\left(e^{-iuk}\phi_T\left(u - \frac{i}{2}\right)\right) \frac{du}{u^2 + 1/4}. \tag{F.1.8}$$

Bibliography

[1] Jim Gatheral, Thibault Jaisson and Mathieu Rosenbaum. Volatility is rough. 2014.

[2] E.Alòs , J.A.Léon and J.Viven. On the short-time behavior of the implied volatility for jump-diffusion models with stochastic volatility. *Finance and Stochastics*, 2007.

[3] Fabienne Comte and Eric Renault. Long memory in continuous-time stochastic volatility models. *Mathematical Finance*, 1998.

[4] Mikkel Bennedsen, Asger Lunde and Mikko S. Pakkanen. Hybrid scheme for Brownian semi-stationary processes. 2017.

[5] Masaaki Fukasawa. Asymptotic analysis for stochastic volatility: Martingale expansion. *Finance and Stochastics*, 2011.

[6] P.Carr and D.Madan. Joint modeling of vix and spx options at a single and common maturity with risk management applications. 2014.

[7] T.Kokholm and M.Stisen. Joint pricing of vix and spx options with stochastic volatility and jump models. *The Journal of Risk Finance*, 2015.

[8] Jim Gatheral, Paul Jusselin and Mathieu Rosenbaum. The quadratic rough Heston model and the joint S&P 500/VIX smile calibration problem. *Mathematical Finance*, 2020.

[9] Giulia Livieri, Andrea Pallavicini and Mathieu Rosenbaum. Rough volatility: Evidence from option prices. 2017.

[10] Masaaki Fukasawa. Volatility has to be rough. 2020.

[11] T. G. Andersen, T. Bollerslev, F. X. Diebold and H. Ebens. The distribution of realized stock return volatility. *Journal of Financial Economics*, 2001.

[12] Mikkel Bennedsen, Asger Lunde and Mikko S. Pakkanen. Decoupling the short- and long-term behavior of stochastic volatility. 2017.

[13] Leonid Mytnik and Eyal Neuman. Sample path properties of Volterra processes. 2011.

[14] Omar El Euch and Mathieu Rosenbaum. The characteristic function of rough Heston models. *Mathematical Finance*, 2016.

[15] Omar El Euch. *Quantitative Finance under rough volatility.* PhD thesis, Université Pierre et Marie Curie, 2018.

[16] Omar El Euch, Mathieu Rosenbaum and Masaaki Fukasawa. The microstructural foundations of leverage effect and rough volatility. 2016.

[17] Kai Diethelm, Neville J.Ford and Alan D.Freed. A predictor-corrector for the numerical solution of fractional differential equations. 2001.

[18] Changpin Li and Chunxing Tao. On the fractional Adams method. 2009.

[19] Masaaki Fukasawa. The normalizing transformation of the implied volatility smile. *Mathematical Finance*, 2012.

[20] Beatrice Acciaio and Julien Guyon. Inversion of convex ordering: local volatility does not maximise the price of VIX futures. 2019.

[21] Julien Guyon. Inversion of convex ordering in the VIX market. 2019.

[22] Aditi Dandapani, Paul Jusselin and Mathieu Rosenbaum. From quadratic Hawkes processes to super-Heston rough volatility models with Zumbach effect. 2019.

[23] Georgiy Shevchenko. Fractional Brownian motion in a nutshell. 2014.

[24] Martin Schmelzle. Option pricing formulae using Fourier transform: Theory and application. 2010.